NUREG/CR-1058
LA-8053-MS
Informal Report

Impact of SIMMER-II Model Uncertainties on Predicted Postdisassembly Dynamics

University of California

LOS ALAMOS SCIENTIFIC LABORATORY
Post Office Box 1663 Los Alamos, New Mexico 87545

NUREG/CR-1058
LA-8053-MS
Informal Report
R7

Impact of SIMMER-II Model Uncertainties on Predicted Postdisassembly Dynamics

C. R. Bell
R. D. Burns III
L. B. Luck

Manuscript submitted: September 1979
Date published: October 1979

Prepared for
Division of Advanced Reactor Safety Research
US Nuclear Regulatory Commission
Washington, DC 20555

UNITED STATES
DEPARTMENT OF ENERGY
CONTRACT W-7405-ENG. 36

TABLE OF CONTENTS

ABSTRACT		1
I.	INTRODUCTION	2
II.	BEST-ESTIMATE CALCULATION OF LOF ENERGETICS	4
III.	SELECTION OF PHENOMENOLOGICAL UNCERTAINTIES	9
IV.	SETTING UP OF THE SIMMER-II CASES	11
V.	ANALYSIS OF THE COMPUTED RESULTS	12
VI.	PHYSICAL INTERPRETATION OF THE RESULTS	14
VII.	CONCLUSIONS	16
APPENDIX A	Basis for the Best-Estimate Analysis	18
APPENDIX B	Characterization of the Uncertainties in Exchange Models	23
APPENDIX C	Design of 15 SIMMER-II Runs with Varied Modeling Assumptions	44
APPENDIX D	Analysis of Variations Among Results of 15 SIMMER-II Runs	50
REFERENCES		58

IMPACT OF SIMMER-II MODEL UNCERTAINTIES ON PREDICTED POSTDISASSEMBLY DYNAMICS

by

C. R. Bell
R. D. Burns III
L. B. Luck

ABSTRACT

The SIMMER-II calculation of the system kinetic energy developed during a voided core postdisassembly expansion in a hypothetical loss of flow (LOF) accident sequence gives results which are more than an order of magnitude below that for an ideal expansion. This work attempts to determine the extent to which uncertainties in the various phenomenological models in SIMMER-II influence the calculated results. A series of 15 separate SIMMER-II calculations were designed to make this assessment. The system kinetic energies which resulted ranged from 2.5 to 20 MJ compared to 100 MJ for the ideal expansion. It is concluded that experimental research in the area of voided core expansions should entail a balance between two areas. First, experiments should be performed that test the major uncertainties in the sequence of events as outlined in this report. Second, in order to increase confidence in the ability of SIMMER to predict other classes of expansions, testing of isolated phenomenological models should proceed.

I. INTRODUCTION

The expansion of the high temperature core materials resulting from core disassembly during an unprotected loss-of-flow (LOF) transient in a Liquid Metal Fast Breeder Reactor (LMFBR) is a complex physical process. The core material undergoes rapid vaporization thereby producing high pressure. This pressure causes the core materials to move very rapidly while at the same time interacting with other fluids and structures. As the core expands, the liquid sodium pool above the core is accelerated upward toward the reactor head. When the sodium pool impacts the reactor head, part of the kinetic energy in the pool is converted to potential energy in the liquid sodium thereby generating large pressures at the reactor head. As a result, the upper reactor vessel and head may be severely loaded. One purpose of the analysis of hypothetical accidents of this type is to determine the structural loadings on the primary system, of which the reactor vessel is a part, and the integrity of the system under these severe conditions.

The SIMMER code series was developed to mechanistically treat the dynamics associated with the "postdisassembly expansion phase" and the "transition phase" of core disruptive accidents in LMFBR's. SIMMER-I[1] was applied to the postdisassembly expansion problem in 1977. Results were substantially less severe than those obtained from idealized expansions. The SIMMER-I analyses[2] were focused on obtaining an understanding of the reduced loads at pool impact with the reactor head. That study was not a sensitivity study in any sense because the major phenomena involved were not quantitatively assessed in the context of a best-estimate calculation. Those results did provide the basis for the more detailed investigation described in this document.

The sensitivity study reported here is based on a specific voided core configuration assumed to follow a severe LOF accident sequence in the Clinch River Breeder Reactor (CRBR). Hence this study provides an in-depth probe into the mechanistic treatment of the expansion phase of only one of the possible accident sequences. This basis was chosen to limit the scope of the study and to make the results more interpretable. Other studies[3] have been performed to investigate the influence of varying initial and boundary conditions on the expansion. All the calculations were performed with SIMMER-II[4] which provides improvements in the models and in operation relative to SIMMER-I.

The possibility of performing sensitivity analysis with large codes like SIMMER-II was first considered about a year ago following similar work in the LWR safety area,[5] when it appeared that useful information could be obtained from a relatively small number of separate code calculations. This is important, since SIMMER is a long-running code (a typical postdisassembly expansion problem requires about one hour on a CDC 7600). A report was prepared outlining a possible approach for applying sensitivity analysis to SIMMER verification.[6] To gain experience with the sensitivity analysis approach, a simplified study of postdisassembly expansion was performed, and the results have been reported.[7] The methods have since been revised and their applicability extended to experiment analysis.[8] The present work is the first attempt to provide comprehensive information about the relative sensitivity of SIMMER-II results for postdisassembly expansion to modeling assumptions in SIMMER-II.

It is possible that such a study could be only marginally useful if the models in the code are improper, deficient, or absent. This circumstance has been recognized and has led to a design for the study that focuses on bounding uncertainties in phenomena as opposed to uncertainties in input data. For example the study considers the total uncertainty in the heat transfer rate between liquid fuel and cladding resulting from transient effects, flow regime effects, radiation, multicomponent effects, material properties, lumped node heat transfer modeling, etc. The intent of this approach is to evaluate whether the modeling assumptions, limitations, and/or deficiencies have a significant effect on the expansion. One limitation of this study (the general approach can accommodate these kinds of variations) is that temporal and spatial variations of modeling uncertainties are not included. If a physical basis exists for the uncertainty in a model or phenomena to change in space and/or time as the expansion proceeds, this study does not reflect this effect. If on the other hand a phenomena is consistently being modeled as too weak or too strong, the study will evaluate its effect on the expansion. Thus a measure of the overall effects of modeling can be obtained whether or not the models themselves are necessarily adequate.

The remainder of this document describes the reference or best-estimate calculation, the selection of phenomenological uncertainties and their ranges, and the setup of the SIMMER-II cases. The results are then analyzed statistically and phenomenologically. The latter is intended to provide some physical

insight into the results of the study. Detailed interpretations and comparisons of the microphysics leading to the range of integral, end-of-transient, results are difficult because of the method of chosing the data used for the different cases. A computer program designed to perform the detailed comparison from the output of the 15 cases is currently being developed. Thus, at the present time, interpretations are based primarily on integral results at the time of head impact. The concluding section of the report describes, in simple terms, the inferences that should be drawn from this study, and the influence this study should have on the planning of experimental research associated with postdisassembly expansion.

II. BEST-ESTIMATE CALCULATION OF LOF ENERGETICS

A best-estimate calculation of an LOF postdisassembly expansion was performed to provide a baseline around which the sensitivity study could be designed. This calculation provides a vehicle for critically evaluating the performance of SIMMER-II on this type of problem and for ascertaining the reasonableness of the predicted results. By carefully studying this calculation we were able to obtain confidence that the calculated behavior was consistent with the modeling assumptions and that basic physical laws were not being violated. This calculation also provided guidance for making prior judgements about the importance of various phenomena to the sensitivity study results.

The best-estimate calculation is based on a geometric model which encompasses the CRBR reactor vessel and its internal structures. This model is discussed in detail in Appendix A. The initial conditions are defined as those resulting from a severe LOF accident sequence which led to essentially complete voiding of the core, upper axial blanket (UAB) and the fission gas plenum (FGP) regions. The accompanying neutronic transient was assumed to result in an average core fuel temperature of 4800 K. The SIMMER-II analysis is initiated at the end of the neutronic transient and before substantial core material motion has occurred. Further details with regard to initial conditions and modeling assumptions are provided in Appendix A.

The physical behavior predicted to occur in this problem is highly complex and interactive. The SIMMER-II treatment is by necessity very complex. An attempt is made below to describe the major events and phenomena that occur

during the expansion. The SIMMER-II results are presented and compared with the SIMMER-I[2] predictions.

The core state following the disassembly phase of the overall accident sequence is one in which the central portion of the core is at high temperature and pressure relative to the peripheral regions. In this particular case the initial pressure gradients are on the order of 25 MPa/m. As a result, the early behavior of the postdisassembly expansion is associated with the rapid redistribution of fuel within the active core region. Within 10 ms the central part of the core has expanded sufficiently to compact the molten core materials to the periphery. The result is a rapid decrease in the peak core pressure as preferential expansion of the hottest two-phase fuel at the core center occurs. As a result of the rapid movement of hot core material into the colder core regions, the hot and cold fuel is calculated to be dynamically mixed to some extent and, because of the SIMMER-II modeling limitations, is assumed to thermally equilibrate instantaneously. This process has been called self-mixing because it is self induced and involves the same material. The degree of self-mixing and the rapidity of thermal equilibration on a core-wide basis is uncertain although it is a real process. Its effect is to transfer energy from the hot fuel to the cold fuel thereby further decreasing the pressure in the core. Another process that occurs in this early time frame is liquid fuel to liquid steel heat transfer. This process is important in further reducing the core pressure. It tends to be amplified in the early part of the expansion as a result of the breakup of the liquid fuel through rapid flashing. The small particle-size, liquid fuel dispersion increases both the area for heat transfer and the conductance of the individual liquid fuel particles. The net effect of these three processes on the core pressure is shown in Fig. 1. In the first 10 ms the core pressure drops from about 27 MPa to 5 MPa. The pressure decay on a longer time scale is the result of continuing heat transfer to the steel in the core and the expansion of the core material into the UAB and FGP regions.

The expansion of the molten core material into and through the upper core structure is a complex process involving phase changes, heat transfer, and momentum transfer. The resistance to the flow of a dense multiphase fluid through the small flow channels of the UAB and FGP is very large. Consequently, these regions strongly limit the rate at which the hot core materials enter the sodium pool at the top of the subassembly region. As the molten

fuel-steel mixture is injected into the UAB and FGP, rapid heat transfer occurs between the molten mixture and the cladding. This results in the ablation of the cladding which in turn adds relatively cold liquid steel to the flowing mixture and enlarges the flow channels. The liquid fuel in the flowing mixture is cooled by heat transfer to the liquid steel with the result that solid fuel particles are formed. The core material also interacts with the thin sodium films that were assumed to remain on the pins in the UCS. Sodium vapor is formed as the sodium is heated. The vapor flows rapidly to the top of the FGP where it initially condenses. Fuel vapor is essentially all condensed on the cold structures or on the cold liquid fuel droplets. By about 20 ms the high void fraction flow of sodium vapor, liquid steel, and solid particulate fuel issuing from the top of the FGP begins to heat the sodium in the transition region (TR) between the FGP and flow guide tubes or upper internal structure regions.

At about 20 ms the movement of the sodium pool begins. The motion of pool from this point on is controlled by the heating of the sodium in the TR. The buildup of pressure in the TR is shown in Fig. 2. The heat transfer from the core materials causes the sodium to generate a maximum pressure of about 1.5 MPa. From Fig. 2 it is seen that the TR pressure decreases very gradually over the term of the expansion. By 100 ms the pressure gradient to drive additional hot material from the core is essentially zero. The heat transfer between the solid fuel particles and liquid sodium and between liquid steel and sodium continues to occur over the remainder of the transient. The two-dimensional character of the TR and the flow area changes that exist between the subassemblies and the flow guide tubes cause residual sodium to remain in the TR for a relatively long time. It is this sodium that continues to vaporize and sustain the vapor pressure shown in Fig. 2.

The sodium vapor expansion zone progresses to the top of the UIS at about 140 ms. From this point on the expansion becomes two-dimensional in the sodium pool. Because the two-dimensional expansion creates volume rapidly, as seen from Fig. 3 showing the cover gas volume as a function of time, the vapor velocities at the exit of the UIS become large (> 100 m/s). A large pressure drop develops between the TR and the expanding bubble that tends to limit the pressure in the bubble to a few tenths of a MPa. At the interface of the expanding bubble the sodium vapor condenses on the colder liquid sodium thereby producing a pressure gradient within the bubble. The net effect is that most

of the expansion (from 140 ms to 260 ms) occurs at an effective driving pressure of about 0.3 MPa. This average pressure produces a kinetic energy of about 5 MJ as the expansion proceeds to about 18 m^3, the effective cover gas volume.

The impact of the sodium pool with the reactor head occurs at about 260 ms and is defined as the time at which the minimum cover gas volume is reached. The maximum kinetic energy in the system always occurs slightly before this time. The surface of the sodium pool is peaked at the center because of the jet-like flow from the UIS. Thus the impact process begins before the cover gas space is filled. As a result the pool kinetic energy begins to be converted to other forms of energy at this earlier time. The system kinetic energy as a function of time is given in Fig. 4. The maximum value is about 5 MJ.

The maximum kinetic energy calculated by SIMMER-II is higher by about 60% than the comparable SIMMER-I value. A variation of this magnitude is not unexpected because the modeling differences between the two versions of the code are substantial and the changes in the geometric model are significant. The results of the sensitivity study discussed in the remainder of this report illustrate the reasons for this difference.

The best-estimate calculation give us an indication of the types of complex, interactive processes that occur in a postdisassembly expansion. Many of these processes or phenomena are competing in terms of their impact on the results. An example of this is associated with the interaction between the hot core material and the above-core pin structure. Rapid heat transfer from the molten material reduces its energy state and therefore its "work potential" but the resulting destruction of the highly resistive pin bundle permits more hot core material to escape to the sodium pool. It is necessary there re to gain an understanding of the uncertainties in these competing phenomena as treated by SIMMER-II and an understanding of the effects of these uncertainties on the calculated results when they are combined in various ways. In addition we need to know which if any of the phenomena and its associated uncertainties play a dominant role in determining the system kinetic energy. This then can provide guidance for further research efforts. The remainder of this document is devoted to determining the impact of uncertainties as they are currently seen for this particular LOF accident sequence.

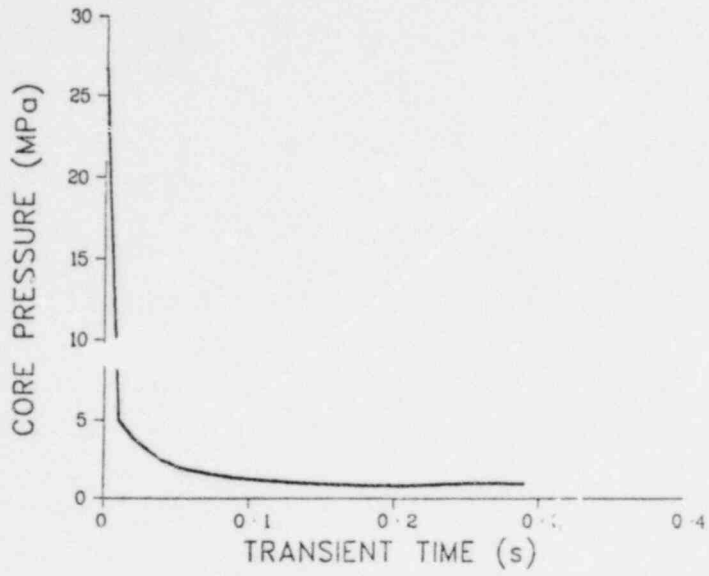

Fig. 1. Core pressure for the best estimate analysis.

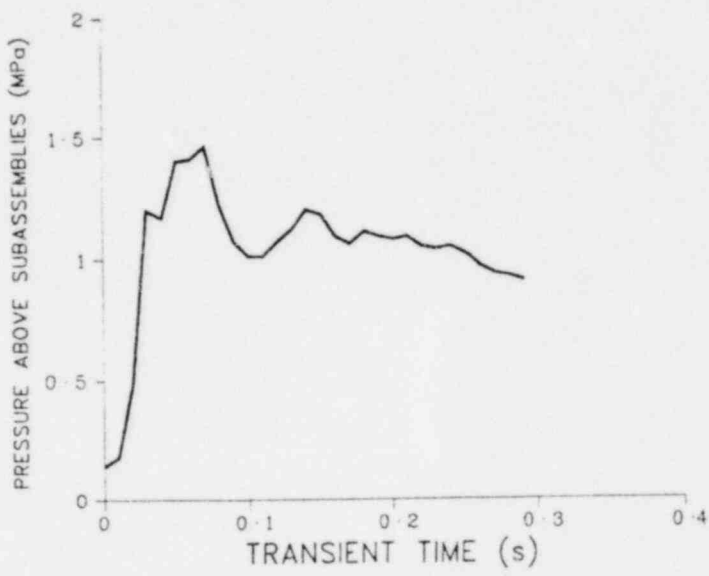

Fig. 2. Pressure above the subassemblies for the best estimate analysis.

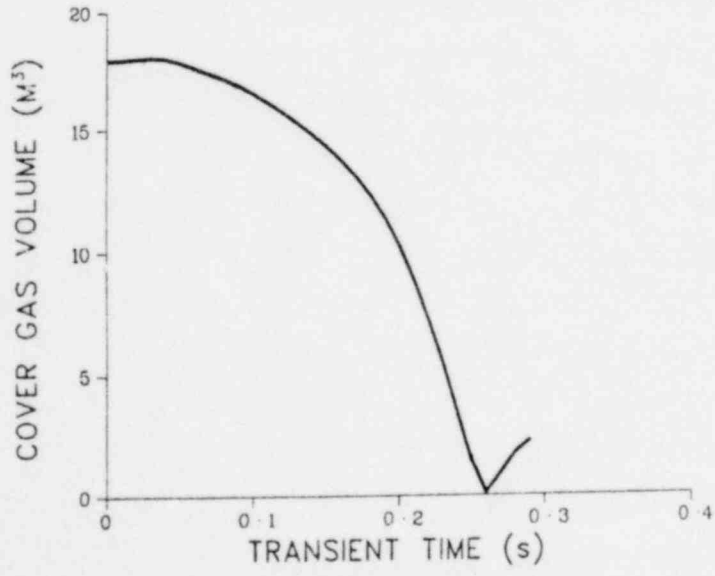

Fig. 3. Cover gas volume for the best estimate analysis.

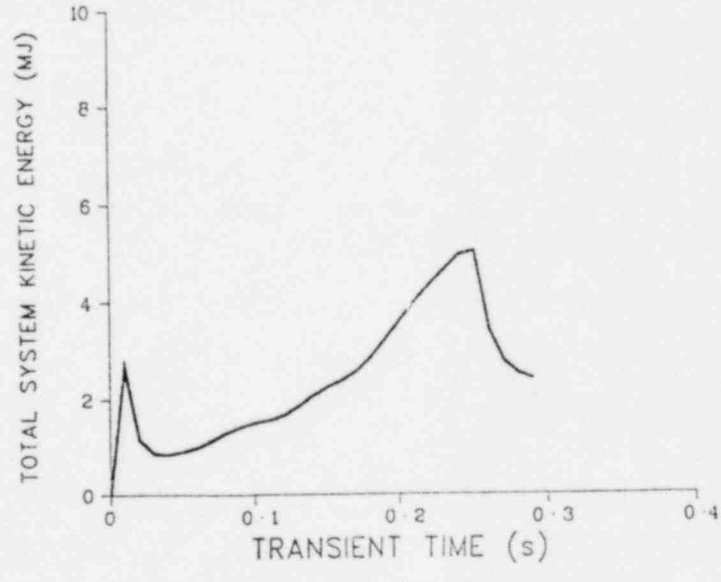

Fig. 4. Total system kinetic energy for the best estimate analysis.

III. SELECTION OF PHENOMENOLOGICAL UNCERTAINTIES

The question of predicting the magnitude of the energetics associated with HCDAs in LMFBR is a very difficult one because it is highly dependent on the accident sequence as well as uncertainties in the treatment of the postdisassembly expansion phase. In analyzing the manner in which SIMMER-II treats the expansion phase and analyzing the basic physics involved, we have identified over 100 contributors to the uncertainty in the prediction of the potential for system damage for a given reactivity ramp rate. These can be separated into four categories.

First there are those contributors to the uncertainty that result from the accident sequence. These are variations and/or uncertainties in the initial conditions and boundary conditions for the postdisassembly expansion phase. These may take the form of material distributions, blockage configurations, disrupted structures, thermodynamic states of the materials, etc.

The second category is associated with uncertainties in the mathematical models used to describe the physics that is believed to occur during the expansion. A particular model may be uncertain for various reasons. First, it may not be representing the fundamental physical configuration correctly. For example, treating a liquid film as liquid droplets in the prediction of the momentum coupling between the liquid and gas fields would clearly be misrepresenting the physics of the situation. Second, the model may not treat all of the interactive characteristics correctly such as dependencies of local conditions and/or the history of the situation. Again the interfield momentum exchange is a good example. The model must attempt to account for the local velocities, the volume fraction of vapor, the dispersion or topology of the liquid and vapors, mixture characteristics of the gases and liquids (and solid particles), the constraining geometry of the flow field, etc. Thus depending on the degree to which these interactive characteristics are modeled correctly, the overall uncertainty in a model can vary in time and space. This is a very difficult type of uncertainty to deal with in terms of its impact on predicted results. Third, a model may be correct in terms of its physics and interactivity, but may simply be consistently too strong or weak. In otherwords it may have a built-in bias. The droplet breakup model is a good example of this type of uncertainty. In general a mechanical stability criteria is used to determine a threshold size. This particular

size is not necessarily a good representative size to use to represent the actual distribution of sizes. Thus a bias is built into the model. In this study the modeling uncertainties (assumed to be all three types) are lumped together and are applied as if they were of the third type. This is an oversimplification but will provide a general indication of the influence of a particular phenomena with an associated uncertainty.

The third category of uncertainties that contribute to uncertainty in the predicted energetics is material properties. This is a large category because in general three or four materials are involved in the expansion, each of which may exist in different physical states. It is a difficult group to deal with in the sense that their uncertainties have indirect and often subtle effects on the expansion. Uncertainty in a simple property such as fuel thermal conductivity can alter the course of the expansion dramatically and perhaps the energetics level. High conductivity will tend to eliminate liquid fuel from the mixture of material which interacts with the sodium above the subassemblies in the best-estimate calculation. This leads to a different behavior in the fuel/steel and sodium interaction phase of the expansion.

The fourth category includes known modeling deficiencies and miscellaneous items such as code operational controls. Some of the modeling deficiencies include a complete flow regime treatment, a definitive interfacial mixing treatment, FCI fragmentation, homogeneous nucleation, and radiation heat transfer.

To deal with all of these contributors in this initial study appeared to be overly ambitious. Further it was desired to maintain a reasonable level of physical interpretability. If the entire set of initial and boundary conditions were included, these would dominate the energetics variations and would tend to mask the influence of other classes of contributors. We concluded that it was appropriate in this study to concentrate on a single accident sequence (severe LOF; completely voided core) and thereby fix the initial and boundary conditions. The material property uncertainties were also eliminated from the study. This large category (48 properties and associated uncertainties) would substantially increase the difficulties of interpretation and their effects would tend to be masked by modeling uncertainties. Because the saturation characteristics are important in determining the driving pressures for the expansion and because their uncertainties are large, this subclass of material properties was included.

The main emphasis of the study then is on the effect of uncertainties in the modeling of the physical processes involved in the expansion.

A total of 28 input parameters that control exchange rates of mass, momentum, and energy and the vapor pressures of fuel, steel, and sodium in the SIMMER-II code were selected for variation. It was determined that to be physically consistent some input parameter values must depend on others (for example, a constant multiplier for structure condensation rate depends on surface area assumed for heat transfer based on flow regime characteristics), and that actually 25 independent input parameters existed. The remaining three could be determined knowing the other 25. These input parameters, the rationale for their selection, and the estimated uncertainties associated with each are described in Appendix B.

The parameter variations represent either direct multiplicative changes in exchange rate correlations or multiplicative shifts in physical characterizations (for example, characteristic size to represent the size distribution from particle breakup). One exception is the variation of the size of the mixing zone for hot core materials and sodium directly above the subassembly region. This variation is accomplished by changing the calculational node size in the mixing region.

IV. SETUP OF THE SIMMER-II CASES

The approach in the study was to perform 15 separate SIMMER runs. The values of the 25 input parameters were simultaneously and independently varied from one run to the next, according to the procedure described in Appendix C. Because the selection of a particular input parameter value varied among the 15 runs in some random pattern (e.g. high in run 1, low in run 2, medium in run 3, etc.), independent of the random patterns associated with the other inputs, it was possible to create many different combinations of simultaneous increases in some exchange rates and decreases in others. In this way interaction among model uncertainties could be studied.

This approach of permitting all uncertain parameters to vary simultaneously provided considerably more information for the same number of runs than the normal type of sensitivity study in which one variable at a time is permitted to change. The random selection of the data sets causes the expansion to occur under conditions in which mitigating effects dominate, amplifying effects dominate, and various combinations in between exist. This

approach also provides a basis from which mathematical statements can be made with regard to the likelihood of having combinations of parameters that would lead to energetics levels greater than those observed in the 15 cases.

V. ANALYSIS OF THE COMPUTED RESULTS

The system kinetic energies at the time the sodium pool begins to impact the reactor head varies between 2.5 and 20 MJ for the 15 cases. The arithmetic average is 8 MJ and the standard deviation is 4 MJ. It is interesting that the average value is different than the best-estimate result of 5 MJ. This is to be expected, however, because all the uncertainty ranges are not symmetric around the baseline values for the imput parameters. Even though the range of results is large, the maximum value of 20 MJ is substantially below the kinetic energy for a consistent isentropic expansion which yields 100 MJ. This study supports the conclusions from the earlier study[2] that the interactive transport processes cause a net mitigation of the energetics for the severe LOF class of expansions even in the context of relatively large uncertainties in the specific treatments of the phenomena involved.

One of the important features of the procedure used in this study is its compatibility with statistical analysis. One important question to be addressed is the likelihood that combinations of the input parameters could yield results greater than 20 MJ if additional calculations were performed. This question is addressed in Appendix D. It is found that if 5% of all possible cases would yield results greater than 20 MJ, then in the 15 cases randomly selected, we had a 50% chance of picking one of them. We know that we did not pick one of these worse cases from the results; therefore, the chance of getting one in a 16th case is only 5%. However, because we only had a 50% chance of picking a worse case in the 15 selected, we can't attach any confidence to our prediction for the additional case. If, however, 18% of all possible cases could yield results greater than 20 MJ, we can say with 95% statistical confidence that we should have seen a worse case in the 15 that were calculated. Because we did not obtain any results greater than 20 MJ, we can say with high confidence that the chance of exceeding 20 MJ on an additional run is not greater than 18%. Thus there is a trade-off between probability and confidence level. The randomness inherent in the procedure used to design this study does permit such a quantification of the meaningfulness of the body of results.

In addition to ascertaining the overall effect of uncertainties in the treatment of the expansion, it is important to determine which, if any, of the phenomena and their associated uncertainties are responsible for the calculated range in system kinetic energy. A correlation method is used that tests for monotonic association between a sequence of input parameter values and the sequence of output values such as system kinetic energy at head impact. The method and its application to this study are described in Appendix D. The determination of the existence of a correlation is based on meeting a statistical criteria that assures to a high confidence level that the apparent correlation is not of a random origin.

The analysis indicates that a strong correlation exists between the dependence of the fuel vapor pressure on fuel temperature and the system kinetic energy. No other statistically significant correlations with a single input variation were found. Variations in the dependence of fuel vapor pressure on temperature results in variations in the initial and transient core pressure. This then is essentially the same as varying the disassembly energetics or the reactivity insertion rate in the LOF accident sequence. The existence of the correlation with fuel vapor pressure is not surprising. It has been independently determined that higher reactivity ramps lead to increased kinetic energy in the best-estimate type analysis.

Further analysis was performed on groupings of parameter variations which were expected to have a common effect on the kinetic energy. Analysis was also performed to determine if correlations exist in particular parts of the fuel vapor pressure uncertainty range. This appears possible because the time frame of the expansion is directly related to the kinetic energy and, therefore, the fuel vapor pressure. These studies show a correlation between the rate of heat loss from the molten fuel and the kinetic energy in the lower part of the fuel vapor pressure range (longer expansion times). If the fuel retains its energy both while in the core and while passing through the upper core structure, it produces more system kinetic energy. This indicates that these heat transfer processes are important primarily in the longer time domain as would be expected. In the short time domain (high fuel vapor pressure range) a correlation appears to exist between phenomena causing large liquid droplet sizes and the system kinetic energy. We believe this correlation to be primarily related to momentum coupling between the liquid and vapor fields. The kinetic energy is reduced as the fields are more tightly coupled.

From the analysis of the results it is apparent that the selection of uncertainty ranges tends to determine to some extent the dominant phenomena in the expansion. As a result, the guidance that this analysis gives to both code development and experimental efforts will tend to change as refinements are made in the uncertainty ranges. It is interesting to note that the strong vapor pressure uncertainty tends to be diminished when the uncertainty is employed consistently through the accident sequence (disassembly phase in addition to expansion phase). High fuel vapor pressure leads to earlier neutronic shutdown in the disassembly phase and therefore reduced initial fuel temperatures for the postdisassembly expansion. The reduced temperatures when combined with the assumed high fuel vapor pressure tends to produce initial core pressures for the expansion that are relatively independent of the fuel vapor pressure assumption. Then if this particular parameter were removed from the study or its uncertainty range substantially reduced, the system kinetic energy variation would be reduced considerably and other uncertainties might dominate the spread in the results. However, the spread may be so small as to be of little practical interest.

VI. PHYSICAL INTERPRETATION OF THE RESULTS

The general characteristics of the LOF postdisassembly expansion in this voided core study do not appear to change greatly as a result of the rather large variations imposed on the phenomena. The basic events described in the best-estimate analysis are present in all cases but, of course, in varying degrees. The core pressure transient is dependent both on the fuel vapor pressure formulation and on the rate of liquid fuel to liquid steel heat transfer in the core. The interaction of the hot core material with the upper core structure is important in all cases although locally large changes in momentum and thermal interactions exist from case to case. In some cases very little liquid fuel exits from the bundles into the sodium pool (solid fuel particles instead) while in other cases the liquid fuel completely traverses the upper core structure. The expansion in all cases is dominated by the rate of sodium vapor production.

The energetics level appears to be primarily dependent on the ability to transport the hot core material into the sodium pool where it can contribute to the rapid generation of sodium vapor. The sensitivity analysis discussed in the preceeding section supports this position. The core pressure is of

fundamental importance in this regard. Heat transfer from the liquid fuel to the liquid steel modifies the core pressure and when coupled to the assumed stratification behavior at heat transfer surfaces tends to control the heat transfer rate to the upper core structure (liquid steel to structure heat transfer is much more effective than liquid fuel to structure). Rapid heat transfer to the structure leads to rapid melting which in turn causes zero momentum steel to appear in the flowing stream, increases in the stream mean density, increases in the local hydraulic diameter, and freezing of the liquid fuel into solid particles. The net result of the combination of large liquid fuel to liquid steel heat transfer and stratified steel at the structure wall is a reduced rate of fuel input to the sodium pool, reduced sodium vapor generation, and reduced kinetic energy.

It is interesting to note that the specific characteristics of heat transfer to the sodium, i.e., both the rate uncertainty and the mixing uncertainty, do not lead to a consistent influence on the system kinetic energy. This would suggest the possibility that over the expansion time interval the ranges of mixing characteristic and local heat transfer rates are causing the available fuel to exert essentially all of its potential influence on the creation of sodium vapor. Then the real physical limitation is again the quantity of fuel and steel injected into the sodium pool. This possibility will be investigated in later work when more detailed processing of the calculated results is completed.

Further analysis is planned that will provide additional information on the exact quantities of fuel and steel exiting the UCS, sodium vapor production rates, overall structure melting rates, etc. This information will aid the physical interpretation substantially.

The primary reason that the spread in system kinetic energy is low, especially when the fuel vapor pressure variation is minimized, is the interaction of multiple mitigating phenomena. The ranges of uncertainties on the mitigators are sufficiently high that in general any one of them is capable of providing a strong mitigating effect on the expansion by itself. With multiple mitigators and a random selection procedure for assigning the strength of mitigation to each, the overall mitigating level can only be low if all mitigations are simultaneously weak. The probability of this occurring is of course much less than if a single mitigator is involved.

One final area deserving discussion has to do with the consistency of the various computed results such as variations in impulse to the head relative to variations in kinetic energy. The results are compiled in Table D-II in Appendix D. We will consider only the maximum and minimum cases, i.e., cases 5 and 12. The maximum and minimum kinetic energies differ by a factor of 8. The impulse, maximum pressure at the reactor head, the maximum average pressure on the head (maximum force) and time to impact all vary by about a factor of 3. All of the latter quantities are related to the velocity of the sodium pool. There should be a square root relationship between kinetic energy and velocity in an ideal, uniform system. The observed relationship appears to be quite close to the ideal. As a result of the calculated consistency, we can be reasonably sure the fluid dynamics of the pool is being analyzed appropriately.

VII. CONCLUSIONS

1. The system kinetic energy developed in a severe LOF, voided core postdisassembly expansion appears to be at least factor of 5 below that for an isentropic expansion even when large phenomenological uncertainties are assumed.

2. The magnitude of the range in system kinetic energy is dominated by the uncertainty in fuel vapor pressure for a particular fuel thermodynamic state in these calculations that are uncoupled from the disassembly calculations. Consistent treatment of this uncertainty through the complete accident sequence would reduce the observed variation in postdisassembly expansion energetics by a large degree (perhaps to 2 to 8 MJ).

3. Because the system kinetic energy for severe LOF, voided core sequences appears to be low and the real effect of modeling uncertainties is small (from conclusion 2), a considerable degree of uncertainty in this analysis can be tolerated without changing the conclusions. Therefore, attempts to better understand the effects of space/time dependencies of phenomenological uncertainties and the effects of combining second level uncertainties (all of those in the treatment of a given phenomena) should be given low priority in terms of voided core postdisassembly expansion.

4. The procedure used in this study provides a methodical assessment of the interaction of uncertainties. The spread in results observed therefore can be taken with higher confidence than obtained by varying one parameter at a time.

5. The procedure provides a basis for quantifying the confidence level in the results obtained. It is estimated that there is a probability on the order of only 10% that combination of uncertainties, as defined, would lead to results larger than those observed.

6. The results obtained are dependent on the selection of uncertainty ranges and on the validity of the SIMMER-II treatment in terms of code framework and completeness. As such the spread in results will change as the uncertainties and the code are refined.

7. Further work in the area of severe totally voided, LOF postdisassembly expansion should be addressed to the question of potential oversights, errors in code framework, and/or errors in designing this study which could change the results in a major way because the margin for uncertainty in this study is large (conclusion 3).

8. Experimental effort directed exclusively toward the area of LOF expansions should be directed at scoping the magnitude of the main mitigating and amplifying phenomena. This is different than performing experiments to provide a detailed understanding and a rigorous modeling basis. Major mitigating and amplifying phenomena are:

   a. structural dynamics of the UCS an UIS,
   b. fluid dynamics of multicomponent, two-phase flow in the UCS,
   c. dynamic meltout of the UCS,
   d. core pressure transient, (self-mixing, fuel-steel heat transfer, fluid topology, fuel vapor pressure),
   e. interactions of fuel and steel with sodium above the UCS, and
   f. recriticality during and following the expansion.

9. A large scale integral experiment would be helpful in satisfying the need outlined in conclusion 7.

10. Emphasis of future work should be on accident sequences involving some sodium in the core at the initiation of the expansion. Because in-core sodium will lead to high core pressures and because high core pressure tends to dominate the energetics (conclusion 2), the real threat to primary system integrity appear to come from these types of accidents.

11. Experimental and modeling efforts should be continued on a more fundamental basis than is required exclusively for the LOF expansion in order to build a general confidence in the predictive capability of SIMMER-II for other accident types and regimes.

APPENDIX A
BASIS FOR THE BEST-ESTIMATE ANALYSIS

The basis for the best-estimate analysis and the sensitivity study was selected to correspond to a particular accident sequence; namely a severe LOF in CRBR. The geometric modeling is consistent with CRBR and the initial conditions are consistent with the selected accident. This basis is essentially the same as that used in previous SIMMER-I analyses[2] of postdisassembly expansion and does therefore provide a continuity between them.

A. Geometric Model

The geometric model shown in Fig. A-1. is based on the CRBR. The model encompasses the entire reactor vessel except for the lower flow module and inlet plenum regions. These regions are ignored because the LOF sequence is assumed to have completely blocked the lower axial blanket and shield regions. Hence the lower portion of the vessel is fluid dynamically isolated from the expansion. The radial region beyond the active core is also assumed to be fluid dynamically insignificant with regard to the expansion and is therefore modeled as a solid steel region. The upper core structure (UCS) and upper internal structure (UIS) are modeled as initially intact. The upper axial blanket (UAB) and the fission gas plenum (FGP) regions are initially 97% voided. The sodium level is assumed to be between the FGP and the transition region (TR). The flow guide tubes in the UIS are modeled as annular channels with a 50% volume fraction set aside a nonparticipating sodium (represent the sodium between the flow guide tubes). The initial heat transfer areas and hydraulic diameters in the UCS and UIS are based on CRBR design data. The cover gas region is set at about 18 m^3 such that this value plus the void in the core, UAB and FGP would total the nominal CRBR cover gas volume of 21 m^3. All structures in this model are treated as rigid members by SIMMER-II. They participate only as heat and momentum sinks and as sources and sinks for liquid materials.

The R-Z numerical model is shown in Fig. A-2. The variable noding feature of SIMMER-II is used to provide better spatial resolution in the regions of greatest activity. The noding in the core is increased from 18 in the SIMMER-I analyses[2] to 120. This is intended to refine the very rapid fluid dynamic behavior in this region and to minimize the numerical "self-mixing" process that was discovered in SIMMER-I. The nodes in the UAB and

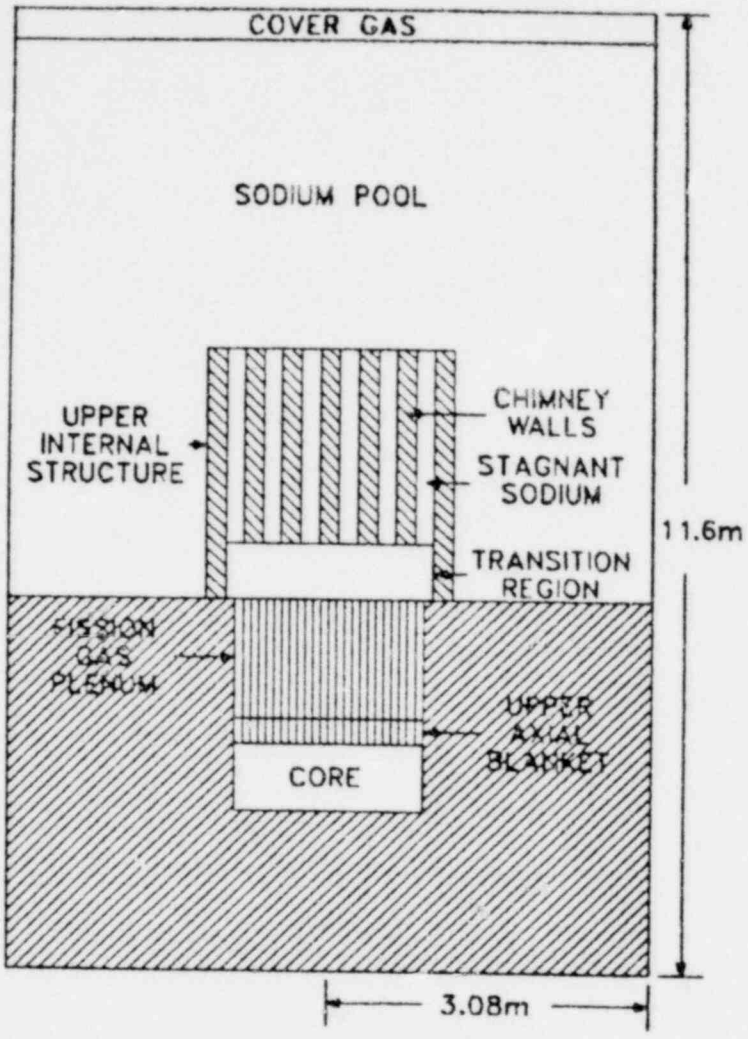

Fig. A-1.
Nominal geometric model postdisassembly energetic analysis.

some in the FGP are made smaller to better define the interactions with these structures. The noding in the TR is also refined as a result of separate effects calculations[9] which showed a dependency of energy transfer between molten core materials and sodium with axial node size. The node size in the TR in effect controls the axial extent of the mixing zone for interaction between core material and sodium. If the zone is small, a small amount of sodium is heated to a high temperature but its work potential is limited. In addition the momentary high sodium vapor pressure tends to limit further interaction. The opposite is true if the nodes are larger. In the nominal or best-estimate calculation, the node size of about 9 cm is selected based on expected particle and liquid droplet penetration depths[9] into a liquid sodium interface.

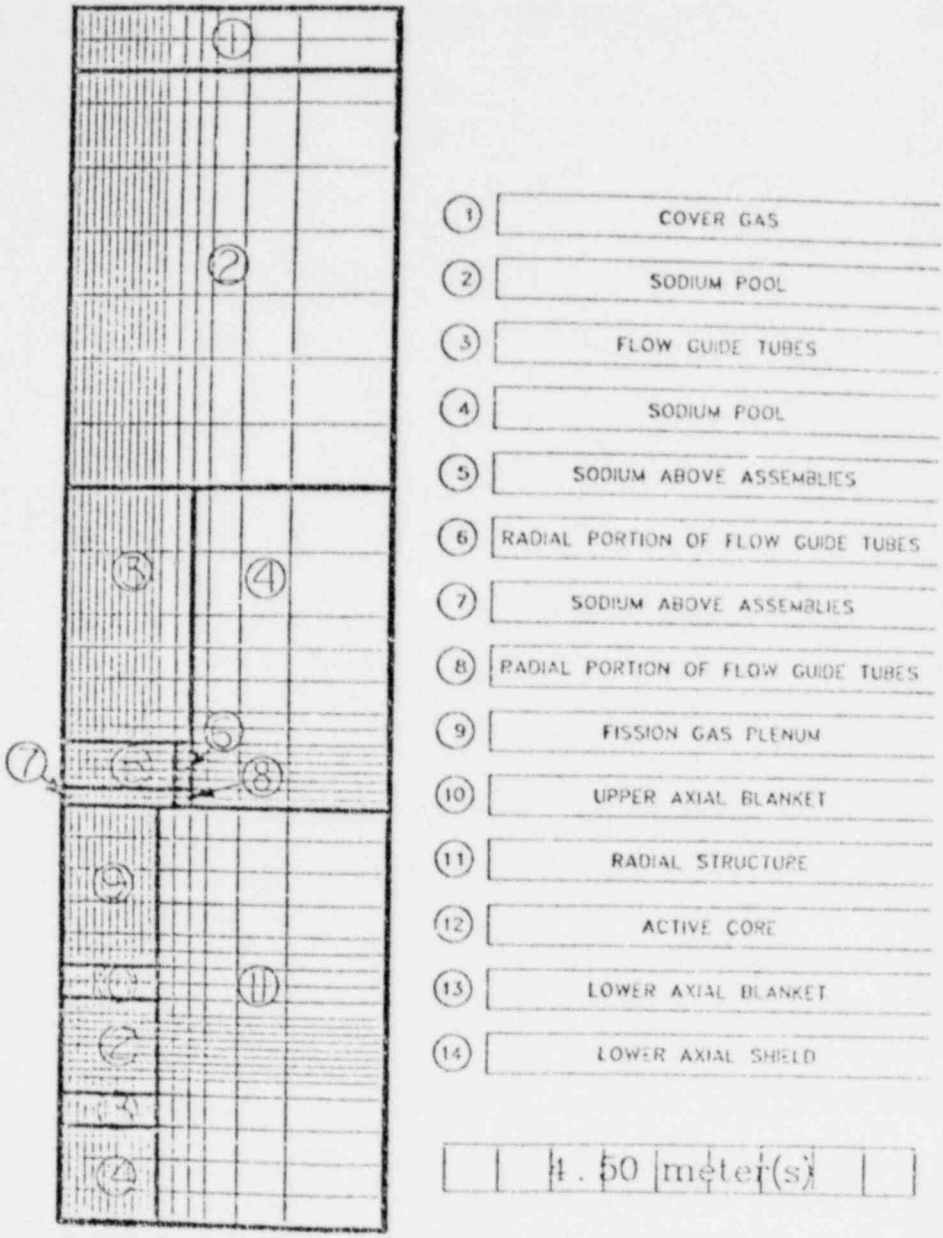

Fig. A-2.
Variable node structure for the LOF postdisassembly expansion.

B. Initial Conditions

The initial conditions for this study are identical to those assumed for the SIMMER-I calculations.[2] The core is assmued to have undergone a severe LOF transient that causes nearly complete voiding of the core, UAB and FGP. It is assumed that substantial clad draining occurs prior to the severe neutronic transient. Therefore the clad steel is not included in the core as a heat sink. The can walls are sssumed to be at the liquidus and to be uniformly distributed throughout the active core. The neutronic transient is assumed to

have brought about an average fuel temperature of 4800 K in the core and to have terminated with minor material displacement. The reactivity insertion rate that produced these conditions was in the range of 50 to 75 $/s.[10]

The initial fuel temperature distribution is peaked at the center of the core as a result of the core power distribution. The maximum temperature is 6020 K while the minimum temperature is 3968 K. The complete initial fuel temperature distribution is shown in Table A-I. The large fuel temperature difference from maximum to minimum produces large initial pressure gradients in the core. The peak pressure at the core center is 26.8 MPa and the minimum pressure at the extreme outer corners of the core is 0.3 MPa. Local saturated equilibrium is assumed between the fuel liquid and vapor at the beginning of the expansion.

Temperatures of the UCS and UIS are assumed to be 1200 K and 1000 K respectively. The fuel temperature in the UAB is taken as 2500 K and the liquid sodium temperature in the TR, UIS, and sodium pool as 1200 K. The initial pressure in all regions except the core is 0.15 MPa.

The cover gas region is modeled with sodium vapor at an initial pressure of 0.15 MPa. In order to maximize the development of systems kinetic energy during the expansion and to avoid the uncertainty associated with the failure of reactor head seals or the potential failure of plugs, it was assumed that the cover gas does not pressurize as the pool rises. Using sodium vapor in this region provides this feature because it condenses as it is compressed and tends to provide an essentially constant pressure above the sodium pool.

Fission gas in the core region is not included explicitly in the calculation. Its effect as a pressure source is not expected to be of major importance because its partial pressure in a released state would be relatively small compared to the pressure levels generated by the fuel and sodium. The major effect of fission gas is more subtle in nature. For example, its presence as a noncondensible gas will subtantially effect the rates of condensation. It may act in a complex way to alter the mixing of core material with sodium above the UCS. It may lead to secondary neutronic transients in the core region because of enhanced radial sloshing. The condensation effect has been considered in separate effects calculation[11] and an attempt to include it is made in this calculation by reducing condensation rates on structure by a factor of 10. The investigation of the other effects of fission gas is being assigned to subsequent analyses.

TABLE A-I

INITIAL FUEL TEMPERATURE DISTRIBUTION (K)

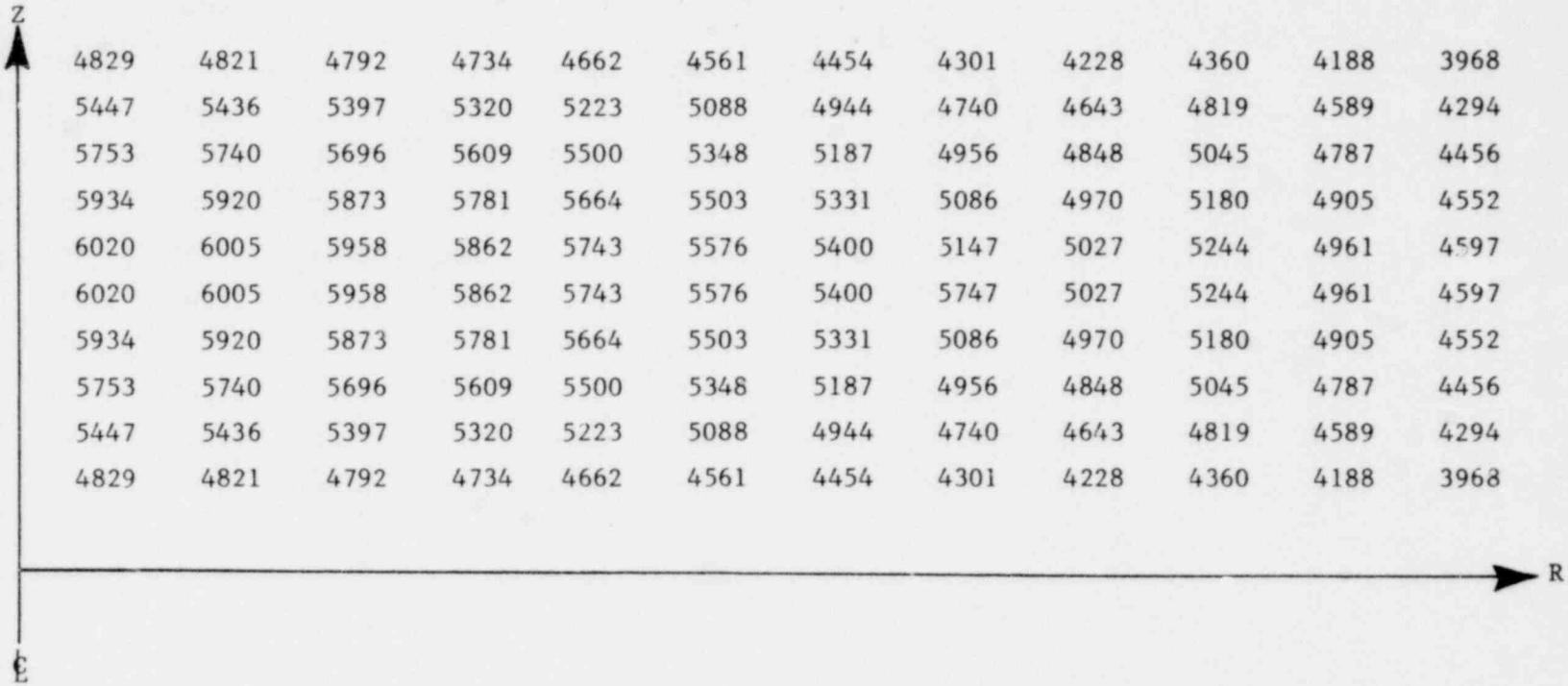

4829	4821	4792	4734	4662	4561	4454	4301	4228	4360	4188	3968
5447	5436	5397	5320	5223	5088	4944	4740	4643	4819	4589	4294
5753	5740	5696	5609	5500	5348	5187	4956	4848	5045	4787	4456
5934	5920	5873	5781	5664	5503	5331	5086	4970	5180	4905	4552
6020	6005	5958	5862	5743	5576	5400	5147	5027	5244	4961	4597
6020	6005	5958	5862	5743	5576	5400	5747	5027	5244	4961	4597
5934	5920	5873	5781	5664	5503	5331	5086	4970	5180	4905	4552
5753	5740	5696	5609	5500	5348	5187	4956	4848	5045	4787	4456
5447	5436	5397	5320	5223	5088	4944	4740	4643	4819	4589	4294
4829	4821	4792	4734	4662	4561	4454	4301	4228	4360	4188	3968

APPENDIX B
CHARACTERIZATION OF UNCERTAINTIES IN EXCHANGE RATE MODELS

SIMMER-II tracks the mass, momentum, and energy, of the LMFBR materials participating in the expansion. It also calculates the amounts of each material in each of the solid, liquid, and vapor phases. The SIMMER-II exchange models determine the exchange rates of (1) mass, through vaporization, condensation, freezing and melting; (2) momentum, through interfield drag and mass transfer; and (3) energy, through conduction and convection heat transfer and through mass transfer. The rates are calculated from mathematical models and correlations which contain various assumptions.

If uncertainties exist in the modeling of exchange processes in SIMMER-II, they are reflected in the calculation of the exchange rates. For example, if the assumed dispersed flow model is used in SIMMER-II when an annular flow model should actually be used, liquid-to-structure heat transfer rates will be underestimated in the code.

Modification of SIMMER-II can be costly, both in terms of making code changes and increasing the running time of the code. Complete experimental verification of the code in all its aspects is also a large and costly undertaking. It is therefore advisable to assess the impact of possible modeling uncertainties and the phenomena in general in a simple manner, if possible, before investing resources in code improvement and specific verification experiments. The approach used in this study to assess the impact of possible uncertainties in exchange rates is to adjust the rates within SIMMER by multiplicative constants to simulate the modeling uncertainties.

The particular models studied include (1) two-phase flow regime, (2) particle size determination, (9) saturation characteristics of LMFBR materials and (3) liquid-liquid heat transfer (4) fluid-structure heat transfer, (5) condensation on structure, (6) interfield drag, (7) characterization of particle size distributions, and (8) characterization of above core mixing. The specific phenomena addressed are shown in the first columns of Table B-I. The rationale for limiting this study to modeling uncertainties and saturation characteristics is discussed in Sec. III. This list of 27 phenomena does not include all the phenomena modeled in SIMMER-II. Some have been deleted from this study because they were found to be unimportant in this type (severe LOF)

TABLE B-I

VARIABLES IN THE POSTDISASSEMBLY ENERGETICS SENSITIVITY STUDY

	Phenomenon	SIMMER-II Variation	Nominal Value	Uncertainty Range	Type of Distribution	Remarks
1.	General flow regime character	Through other parameters	1	$0.1 \le x_1 \le 10$	Logarithmic	x_1 small is dispersed regime
2.	Multicomponent stratification effect	Through other parameters	0.5	$0 \le x_2 \le 1$	Linear	x_2 small indicates liquid fuel at walls
3.	Heat transfer from liquid fuel to structure	Multiplying constant in the liquid fuel convective heat transfer correlation	$y_1 = 0.023$	-	-	$y_1 = 0.023\ x_1\ (1-x_2)$
4.	Heat transfer from liquid steel to structure	Multiplying constant in the liquid steel convective heat transfer correlation	$y_2 = 0.025$	-	-	$y_2 = 0.025\ x_1 x_2$
5.	Heat transfer from liquid sodium to structure	Multiplying constant in the sodium-to-steel convective heat transfer correlation	$y_3 = 0.025$	$0.5 \le x_3 \le 2$	Logarithmic	$y_3 = 0.025\ x_3$
6.	Heat transfer from vapor mixture to structure	Multiplying constant in the vapor-to-steel convective heat transfer correlation	$y_4 = 0.023$	$0.33 \le x_4 \le 3$	Logarithmic	$y_4 = 0.023\ x_4$
7.	Structure condensation rate	Fraction of structure area available for condensation	$y_5 = 0.1$	-	-	$y_5 = 0.1(1 - x_1/10)$
8.	Heat transfer between vapor mixture and liquid droplets	Multiplying constant in the liquid-to-vapor heat transfer correlation	$y_6 = 0.37$	$0.33 \le x_5 \le 3$	Logarithmic	$y_6 = 0.37\ x_5$
9.	Heat transfer between liquid fuel and liquid steel	Multiplying coefficient on the liquid fuel-to-liquid steel heat transfer	$y_7 = 0.2$	$0.2 \le x_6 \le 5$	Logarithmic	$y_7 = 0.2\ x_6$
10.	Heat transfer between liquid fuel and liquid sodium	Multiplying coefficient on the liquid fuel-to-liquid sodium steel heat transfer	$y_8 = 100$	$0.1 \le x_7 \le 5$	Logarithmic	$y_8 = 100\ x_7$
11.	Heat transfer between liquid steel and liquid sodium	Multiplying coefficient on the liquid steel-to-liquid sodium steel heat transfer	$y_9 = 1$	$0.1 \le x_8 \le 5$	Logarithmic	$y_9 = x_8$
12.	Heat transfer between liquid sodium and solid fuel particles	Multiplying coefficient on the liquid sodium-to-solid fuel particle heat transfer	$y_{10} = 1$	$0.2 \le x_9 \le 5$	Logarithmic	$y_{10} = x_9$

TABLE B-I (cont)

	Phenomenon	SIMMER-II Variation	Nominal Value	Uncertainty Range	Type of Distribution	Remarks
13.	Heat transfer between liquid sodium and solid steel particles	Multiplying coefficient on the liquid sodium-to-solid steel heat transfer	$y_{11} = 1$	$0.2 \le x_{10} \le 5$	Logarithmic	$y_{11} = x_{10}$
14.	Fluid friction between liquid and structure	Multiplying constant in the liquid friction factor correlation and input minimum friction factor	$y_{12} = 0.08$ $y_{13} = 0.008$	$0.33 \le x_{11} \le 3$ $0.75 \le x_{12} \le 1.25$	Logarithmic Logarithmic	$y_{12} = 0.08\ x_{11}$ $y_{13} = 0.008\ x_{12}$
15.	Fluid friction between vapor mixture and structure	Multiplying constant in the vapor friction factor correlation and input minimum friction factor	$y_{14} = 0.08$ $y_{15} = 0.008$	$0.33 \le x_{13} \le 3$ -	Logarithmic	$y_{14} = 0.08\ x_{13}$ $y_{15} = 0.008\ x_{12}$
16.	Two-phase flow effect on fluid friction	Two-phase pressure drop field weighting factor	$y_{16} = 0.5$	-		$y_{16} = 0.444\ x_1 + 0.056$ if $x_1 < 1$ $y_{16} = 0.5 + \ln x_1$ if $x_1 \ge 1$
17.	Drag between liquid and vapor	Drag coefficient and exponent on the vapor volume fraction	$y_{17} = 0.5$ $y_{18} = 3.5$	$0.5 \le x_{14} \le 2$ $0 \le x_{15} \le 5$	Logarithmic Linear	$y_{17} = 0.5\ x_{14}$ $y_{18} = x_{15}$
18.	Fluid dynamic droplet breakup	Critical Weber number	$y_{19} = 22$	$0.2 \le x_{16} \le 2$	Logarithmic	$y_{19} = 22\ x_{16}$
19.	Liquid-liquid heat transfer in single-phase liquid regions	Maximum liquid droplet radius	$y_{20} = 0.001$	$0.5 \le x_{17} \le 2$	Logarithmic	$y_{20} = 0.001\ x_{17}$
20.	Liquid coalescence	Coalescence coefficient	$y_{21} = 1$	$0.1 \le x_{18} \le 10$	Logarithmic	$y_{21} = x_{18}$
21.	Liquid droplet size distribution representation	Multiplying constant on the internally calculated droplet size	$y_{22} = 1$	$0.5 \le x_{19} \le 2$	Logarithmic	$y_{22} = x_{19}$
22.	Solid fuel particle size distribution representation	Direct input	$y_{23} = 0.0001$	$0.5 \le x_{20} \le 2$	Logarithmic	$y_{23} = 0.0001\ x_{20}$
23.	Solid steel particle size distribution representation	Direct input	$y_{24} = 0.001$	$0.5 \le x_{21} \le 2$	Logarithmic	$y_{24} = 0.001\ x_{21}$
24.	Fluid mixing in the transition region	Node size in the transition region	$y_{25} = 0.087$	$0.0508 \le x_{22} \le 0.3048$	Linear	$y_{25} = x_{22}$

TABLE B-I (cont)

	Phenomena	SIMMER-II Variation	Nominal Value	Uncertainty Range	Type of Distribution	Remarks
25.	Vapor pressure of fuel	Multiplying constant in the fuel vapor pressure correlation	$y_{26} = 1.44(10^{11})$	$0.5 \leq x_{23} \leq 4$	Logarithmic	$y_{26} = 1.44(10^{11})x_{23}$
26.	Vapor pressure of steel	Multiplying constant in the steel vapor pressure correlation	$y_{27} = 1.34(10^{11})$	$0.5 \leq x_{24} \leq 4$	Logarithmic	$y_{27} = 1.34(10^{11})x_{24}$
27.	Vapor pressure of sodium	Multiplying constant in the sodium vapor pressure correlation	$y_{28} = 3.76(10^{9})$	$0.9 \leq x_{25} \leq 1.1$	Linear	$y_{28} = 3.76(10^{9})x_{25}$

of postdisassembly expansion. Heat transfer between solid fuel and solid steel particles is an example. In the best-estimate analysis these solid particles did not coexist to any significant extent and could not have a major influence regardless of the uncertainty in the heat transfer rate between them. The list in Table B-I represents the phenomena which have been delineated from the best-estimate analysis as having a major or potentially major impact on the course of the expansion.

The vehicles in SIMMER-II that are used to carry the phenomenological uncertainties into the interactive analysis are shown in the second column in Table B-I. Several of the entries require some explanation. Phenomena 1 and 2, flow regime character and multicomponent preference, do not directly enter the calculation but instead modify the uncertainties in other phenomena such as liquid fuel and steel heat transfer to the upper core structure (UCS). Liquid sodium heat transfer to structure is not included as a vehicle for flow regime and multicomponent uncertainties because in this study very little energy flows through this path (UCS initially voided and heat transfer area in the upper internal structure (UIS) is small). The flow regime uncertainty also influences the structure surface area exposed for condensation and direct vapor heat transfer to the surface and influences the two-phase pressure drop partition between the liquid and vapor fields. A direct coupling between the flow regime uncertainty and the momentum coupling between the liquid and vapor fields was not made. It was not clear how to construct a simplistic coupling in a rod bundle geometry where wavelet/film flow may have as large an interfield coupling as dispersed, liquid droplet flow with small droplets.

We turn now to the approach used to establish the range of uncertainties for each phenomenon and the interpretation of the physical uncertainties into SIMMER-II uncertainties. The physical uncertainties were established by first listing all aspects of a given phenomenon (exchange process), as it is expected to occur in this application, which may contribute to the uncertainty. These may be transient effects, geometric effects, flow topology effects, distribution effects, material property uncertainties, multicomponent effects, interference effects such as heat transfer to a surface that is melting, empirical correlation uncertainty, radiation effects, droplet-droplet interaction characteristics, etc. After identifying these contributors for each phenomenon, an attempt was made to

determine limiting contributors thus providing a basis for establishing the uncertainty ranges without analyzing each contributor in detail. The numerical values assigned to the ranges depend on the SIMMER-II vehicle for incorporating each variation. In most cases the phenomenological uncertainty is applied as a multiplicative factor on the SIMMER-II model for that phenomenon. For example, heat transfer from liquid fuel to solid cladding is controlled by both the convective heat transfer coefficient for the fuel and the internal resistance of the cladding. If the overall thermal resistance is dominated on the average by the liquid fuel, the overall uncertainty in this phenomena can be incorporated into SIMMER-II as a variation or uncertainty in the liquid fuel heat transfer coefficient alone. Considerable care must be used in generating the SIMMER-II variation to assure that the true desired influence on the phenomena of interest is being effected.

This important aspect of assigning uncertainty ranges has to do with averaging uncertainties in time and space. Consider for example the influence of fuel crust formation at a surface on the heat transfer from liquid fuel to that surface. The heat transfer rate is greatly affected by the stability of the crust, i.e., whether it remains in place. There is considerable uncertainty related to the stability of crusts of this type in a postdisassembly expansion environment and therefore considerable uncertainty in the associated heat transfer phenomenon. If crust formation is expected to occur over a time interval that represents only a fraction of the time over which this phenomenon occurs or crust formation occurs in only a small region relative to the region in which the phenomenon occurs, the uncertainty in the phenomenon on the average is much less than the local or temporal uncertainty. The modification of the local uncertanties to represent average uncertainties is accomplished primarily by informed judgment. This is another way in which a thorough understanding of the best-estimate analysis is helpful in designing a study of this type.

In the remaining portion of this Appendix each phenomenon will be considered in detail in terms of defining the associated uncertainties. A summary of the ranges is given in the fourth column of Table B-I. The baseline or best-estimate value of the SIMMER-II input parameters carrying the variations is given in the third column. Finally the manner in which the uncertainties are applied in relation to the baseline values is shown in the last column of Table B-I.

A. Liquid to Structure Heat Transfer

We will consider first the heat transfer between liquid fuel and structure and liquid steel and structure. The LOF postdisassembly expansion the steel structure in the core region is assumed to be at its melting point and the fuel is completely molten. The upper axial blanket (UAB) and fission gas plenum (FGP) regions are initially voided of sodium but are assumed to have intact pins and subassembly can walls. Because the structure surface area in these above core regions is large, because the hot core materials are forced through these regions thereby permitting the heat transfer phenomena to occur, because the melting of the pin structure changes the throttling characteristics of these regions, and because the characteristics of the liquid material exiting the subassemblies and interacting with the sodium may strongly affect the energetics, the uncertainties in these two phenomena (3 and 4 in Table B-I) are believed to be important and to be effective primarily in the local region of the upper core structure (UCS), i.e., the UAB and FGP regions.

Figure B-1 gives a visualization of the environment in which these phenomena are occurring. A two-phase, two component fluid flows past the surfaces in a transient manner. The distribution of material along the flow path is nonuniform and transient as shown schematically in this Fig. Heat is transferred to the wall where melting may be occurring and crusts may be forming, all in a transient manner. As materials melt and/or freeze the flow channel dimensions change. This is a very complex environment and is even more so when the other concurrent phenomena such as internal pin heat transfer, condensation, fission gas release, et ., are included.

In Table B-II we list the aspects of these heat transfer modes that introduce uncertainties with regard to the SIMMER-II representation.[4] A problem arrives in dealing with a number of contributors such as these in Table B-II. That problem is associated with the degree of independence of the contributors. We have elected in this study to set the bounding uncertainties from the bounding contributor and to assume that all combinations of contributor are, on the average, within these bounds. Going beyond this level of detail is in the same class as tracking temporal and spatial variations in the uncertainties, both of which are not addressed in this study.

The lower bound on the uncertainty is controlled by the multicomponent stratification. Complete stratification in the limit of a single-phase liquid flow would drive the direct heat transfer between the liquid in the core of

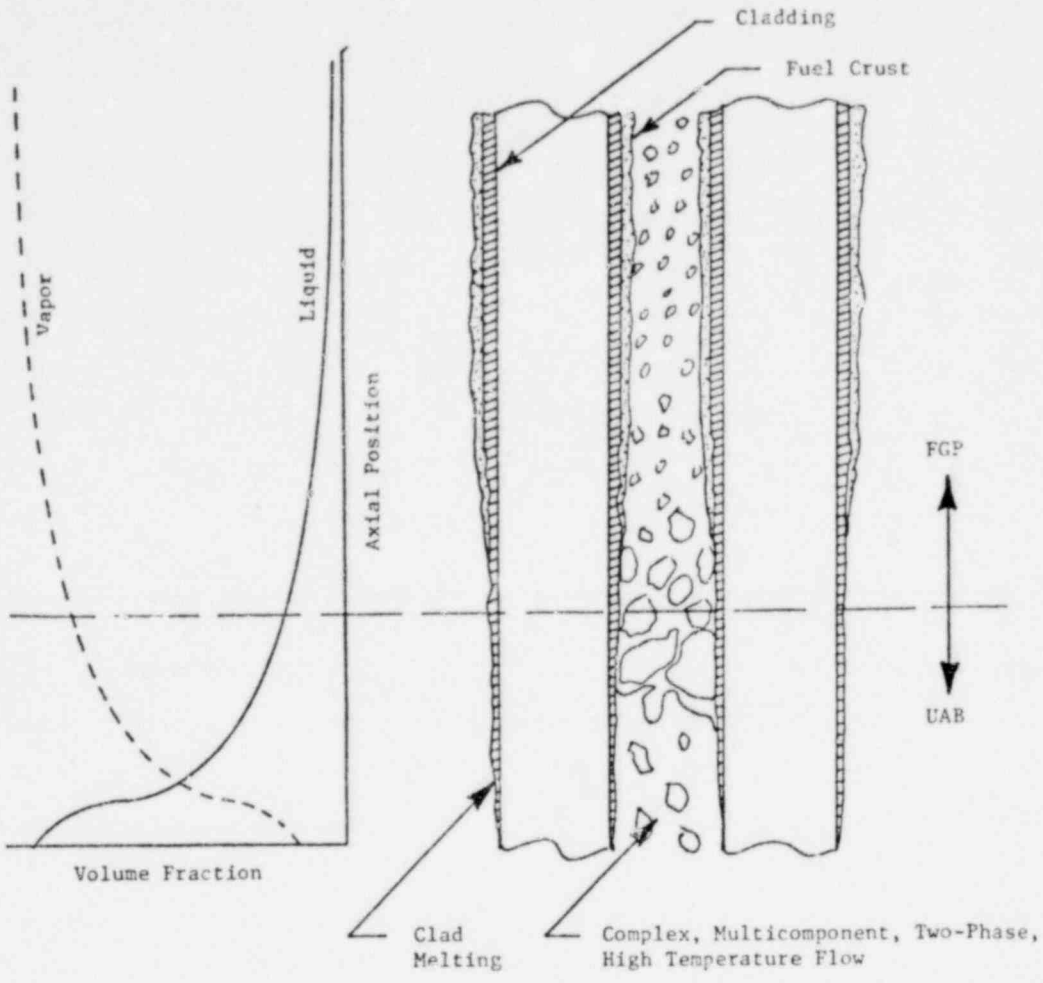

Fig. B-1.
Visualization of the environment for liquid fuel and liquid steel heat transfer to structure.

the stream and the wall to zero. Because the stratification could be in either order, i.e., liquid fuel at the wall or liquid steel at the wall, both heat transfer phenomena have a zero lower limit. A stratification parameter was defined (x_2 in Table B-I) such that as it varied from 0 to 1 the stratification or preferential association of liquid with the wall would vary from liquid fuel only to liquid steel only.

We believe the upper bound on these two heat transfer phenomena is controlled by the flow regime characterization. SIMMER-II does not attempt to track a classical flow regime characterization of the flow. It treats only a dispersed flow topology with various modifications to approach the bubbly flow (low vapor volume fraction) limit. In this complex and transient environment the true fluid topology is highly speculative. In order to provide a systematic variation in the flow topology and therefore the phenomena which depend

TABLE B-II

CONTRIBUTORS TO UNCERTAINTIES IN LIQUID FUEL AND LIQUID STEEL HEAT TRANSFER TO STRUCTURE

	Contributors	Remarks
1.	Transient Flow	Effect may be similar to entrance region of a channel.
2.	Flow Regime	Tends to determine the degree of liquid contact with the surface.
3.	Multicomponent Flow	May lead to stratification.
4.	Transient Heat Transfer	The lumped node formulation of SIMMER-II will be in error under rapid transients and thick walls.
5.	Empirical correlations for convective heat transfer coefficient.	May not be applicable for the materials under these conditions.
6.	Simultaneous Surface Melting	Tends to alter the thermal resistance in the melting body and may generate a stratified layer of melt. May alter the effective heat transfer coefficient in the stream.
7.	Material Properties	Mainly, concern is with fuel thermal conductivity.
8.	Fuel Crust Stability	Tends to be localized near top of FGP where fuel begins to freeze in bulk. May occur locally (boundary layer) over entire region.
9.	Radiation	Not included explicitly in SIMMER-II.

on it, a simple procedure is employed which causes the liquid or vapor preference for contact with the wall to vary. This is a generic way to span the flow topology from fully dispersed (vapor continuous with little liquid contact with the walls) to film annular (no vapor in contact with the wall). This procedure would not be physically appropriate for low vapor volume fraction flows unless vapor blanketing were a real possibility. This is not a problem in this study because the flow in the UCS is on the average characterized by a relatively high vapor volume fraction.

To set the numerical magnitudes of the parameter for flow topology (flow regime), we must remember that the SIMMER-II model applies a liquid volume fraction weighting factor to the liquid-structure heat transfer. The simple physical interpretation is that the phenomenon will be stronger (higher heat transfer rate per unit surface area) if more material is in the channel because of a higher likelihood of liquid-surface contact. A typical average flow of material in the UCS for the best-estimate analysis is about 10 volume percent liquid and 90 volume percent vapor. Hence SIMMER-II would calculate a heat transfer rate based on a liquid-structure contact area of 10% of the actual structure area. In order to force SIMMER-II to calculate the heat transfer as if full liquid-structure contact existed (film flow), the thermal resistance would have to be decreased by a factor of 10 or in this case the heat transfer coefficients for liquid fuel and steel would be increased by a factor of 10. An equivalent 1% contact would be achieved (fully dispersed) if the input heat transfer coefficients are reduced by a factor of 10. The range for the flow regime parameter (x_1 in Table B-I) was taken as 0.1 to 10 thereby spanning the topology range for the average flow conditions.

The input heat transfer coefficients for liquid fuel and steel are calculated as shown in the fifth column of Table B-I. The input parameters y_1 and y_2 are functions of both the multicomponent parameter, x_2, and the topology parameter x_1. As can be seen from the expressions, large values of x_1 favor liquid-structure heat transfer.

The uncertainty range for liquid sodium to structure heat transfer in this study is not nearly as wide as for fuel and steel. The phenomena occurs primarily in the upper internal structure (UIS) which has a small surface area and is expected to have a rather small effect on the expansion. The heat transfer occurs primarily as the expansion bubble interface passes through the UIS. From that point on the flow should be dispersed as a result of the high vapor velocities (> 100 m/s). Because this phenomenon occurs in a much less complex environment and is of lesser importance, an uncertainty range of 0.5 to 2 times the best-estimate representation was assumed.

B. Vapor to Structure Heat Transfer

The uncertainty range for heat transfer between vapor and structure was established in the same way as for the liquids. The items listed in Table B-II generally apply except for the addition of a contributor associated with simultaneous condensation. This heat transfer process is calculated as a part

of the structure condensation model. It is through the condensation model that the flow regime effect enters this heat transfer mode (item 7 in Table B-I). We estimate that the uncertainty in the empirical correlation for the heat transfer coefficient dominates the range. This results primarily from the uncertainty in vapor mixture properties. A range of 0.33 to 3 times the best-estimate representation was selected.

C. Condensation on Structure

The structure area available for structure condensation (item 7 in Table B-I) is strongly flow regime dependent. To provide a consistent influence of flow topology, the variations in this area should be directly related to the flow regime parameter discussed above. The simple formulation given in Table B-I provides the desired coupling. The baseline value of 0.1 is used to weaken structure condensation as predicted by SIMMER-II (heat transfer controlled only) in order to represent the effects of noncondensible gases and multicomponent vapors. Other contributors to the uncertainty in structure condensation are believed to be within the limits established by flow regime considerations.

D. Vapor to Liquid Heat Transfer

The vapor-liquid heat transfer phenomena has a number of contributors to its uncertainty as shown in Table B-III. There does not appear to be obvious bounding contributors in this list. The droplet size distribution effect (single size used in SIMMER-II) could be large but because it will be varied directly (items 21 through 23 in Table B-I) it is removed from further consideration here. The heat transfer correlation can be uncertain as it is applied to situations with various vapor volume fractions. The baseline representation uses a single particle in a free stream as a basis. Correlations for particle beds may increase the heat transfer coefficient by on the order of a factor of 3. The flow topology is again important. The region in which this mode of heat transfer is strong is in the UCS where the temperature differences are large. As discussed above the flow topology in this region can be visualized as film or dispersed in the extremes. For the average flow conditions of 10% liquid in the channel and droplet radii of about 0.001 m the liquid surface area per unit volume of UCS in the dispersed limit is 15 m^2/m^3. If all the liquid is as a film on the structures, the liquid surface area is on the order of 400 m^2/m^3. Hence a factor of three uncertainty due to flow regime or topology is not unreasonable. The overall

TABLE B-III

CONTRIBUTORS TO THE UNCERTAINTY IN THE VAPOR TO LIQUID HEAT TRANSFER

	Contribution	Remarks
1.	Empirical Correlation	Depend on vapor mixture properties and degree of droplet-droplet interference.
2.	Simultaneous Phase Change	Vaporization and condensation changes boundary layer gradients and concentrations in the vapor mixture.
3.	Droplet Size Distribution	SIMMER-II uses one size to characterize the distribution.
4.	Transient Heat Transfer	SIMMER-II is quasistatic.
5.	Material Properties	High temperature vapors.
6.	Radiation	Not included in SIMMER-II.
7.	Transient Flow	Developing boundary layer effects.
8.	Flow Regime	Changes interfacial area, relative velocity, and correlation validity.

range was taken as 0.33 to 3 times the baseline representation. Note that the variation is being incorporated through the vapor heat transfer correlation. This will in fact cause the entire phenomenon to vary because it controls the magnitude of the overall thermal resistance.

E. Liquid to Liquid and Liquid to Particle Heat Transfer

The droplet-droplet and droplet-particle heat transfer phenomena are all similar in terms of the uncertainties involved. We will therefore discuss them as a group (items 9 through 13 in Table B-I). The various contributors to the uncertainty ranges are listed in Table B-IV. Again the droplet and particle size distribution effects are treated as separate parameters. The primary candidates for bounding the ranges are believed to be the transient heat transfer effect, flow regime effect, and contact times. Because contact times are expected to be less than a millisecond it is expected that the quasistatic, lumped node heat transfer representation used in SIMMER-II may underestimate the heat transferred per contact by on the order of a factor of 5. On the other hand the time of contact is

TABLE B-IV

CONTRIBUTORS TO THE UNCERTAINTY IN LIQUID-LIQUID LIQUID-PARTICLE HEAT TRANSFER

	Contributors	Remarks
1.	Droplet and particle size distributions.	SIMMER-II used one size to characterize the distribution.
2.	Flow Regime	Film flow forces direct contact.
3.	Miscibility of Liquid	Model assumes that liquids are completely separate.
4.	Transient Heat Transfer	Contact times are short.
5.	Contact Area	Depends on deformation of droplets during impact.
6.	Contact Time	Complex function of impact mechanics and initial relative velocities.
7.	Vaporization at Contact	In general this occurs only when sodium is present.
8.	Radiation	Not included in SIMMER-II.
9.	Material Properties	Mainly fuel conductivity.
10.	Freezing at Contact Point	

probably overestimated in the SIMMER-II model and could easily cause a reduction in the heat transfer per contact by on the order a factor of 5. This is a case where there is some physical rationale for two contributors to be coupled. The flow regime effect can cause considerable uncertainty in these direct contact heat transfer modes. If all the liquid is constrained to a film, there is forced contact between the materials just as there would be in low vapor volume fraction flow. The flow regime effect is primarily important in the UCS where the liquid fuel-liquid steel mode is dominate. We estimate that on the average the uncertainty in these phenomena is on the order of 0.2 to 5 times the baseline representation. Special cases occurs for the liquid fuel-sodium and liquid steel-sodium phenomena. If the temperatures are sufficiently high, it may be possible to generate vapor blanketing which would further retard the heat transferred per contact. In these two phenomena the lower limit of the uncertainty ranges was further reduced to 0.1.

The baseline value used for item 10 in Table B-I is 100 instead of 1. This value causes the liquid fuel to sodium heat transfer rate to be characteristic of one involving fuel particles of radii equal to .0001 m when SIMMER-II calculates fuel droplets of 0.001 m in radius. Thus we are attempting to force the heat transfer rate to reflect fuel fragmentation.

F. Fluid to Structure Momentum Coupling

The contributor to the uncertainty range for the momentum coupling between liquids and structures are listed in Table B-V. We are considering at this point the situation where liquid alone is flowing in the channel. The two-phase effects are addressed below. Again this process is primarily important in the UCS where the multicomponent flow is made up of liquid fuel, liquid steel and solid fuel particles. We believe that the bounding contributor is the transient flow effect which we estimate to be represented by a range of friction factors equal to 0.33 to 3 times the classical friction factor.

The contributors to the uncertainty range for the momentum coupling between single phase vapor and structure are also given by Table B-V. The transient flow effect is believed to dominate the uncertainty range for this coupling also and the limits are set at 0.33 and 3 as above.

In both of these latter two phenomena the roughness effect has been treated separately because it sets a lower bound on the magnitude of the friction factor in the high Reynolds number range. This bound is also uncertain to some degree because of changes in surface conditions when melting occurs and because of transient hydraulic diameter effects. We believe that realistically the uncertainty range is from 0.24 to 1.25 times the baseline value of 0.008. The biasing in the smaller direction reflects the assumed surface smoothing as surface melting occurs.

G. Two-Phase Flow Effects on Fluid to Structure Momentum Coupling

The normal treatment of the fluid-structure interaction in two-phase flows is to relate the two-phase pressure drop to that which would exist if one or other of the phases alone were flowing in the channel. This approach is used in SIMMER-II but an additional piece of information is required that is normally not considered. This has to do with the manner in which the two-phase pressure drop is partitioned between the vapor and liquid fields. In general, we would expect the flow topology to have a great deal to do with this partitioning. The interfield drag or momentum coupling between the

TABLE B-V

CONTRIBUTORS TO THE UNCERTAINTY RANGES FOR

SINGLE-PHASE FLUID TO STRUCTURE MOMENTUM EXCHANGE

	Contributors	Remarks
1.	Transient Flow	
2.	Complex Flow Channel	Wire wrap pin bundle.
3.	Multicomponent	Could be severe for liquids.
4.	Area Changes	Changing dynamically as pins melt and liquids freeze.
5.	Surface Characteristic	Roughness.
6.	Cross-flow effects	
7.	Material Properties	
8.	Effects of Solid Particles	
9.	Simultaneous Freezing and Melting	Local stratification.
10.	Friction Factor Correlation	Changes with Re number.

liquid and vapor fields also plays a role in the two-phase pressure drop. In the limit of completely dispersed flow we would expect the direct influence of the wall on the liquid field to be at a minimum. In the other extreme of the liquid being at the wall (film or low vapor volume fraction flow), the wall would have very little direct influence on the vapor field.

The preferential influence of the structure on either the vapor or liquid field is viewed as an uncertainty in the flow resistance produced by the structures. This effect is incorporated in SIMMER-II ough a two-phase pressure drop weighting factor, y_{16} (Table B-I). It is incorporated in a way that produces liquid-structure preference when y_{16} is 1 and vapor-structure preference when y_{16} is small. This parameter is considered to be related directly to the flow regime parameter, x_1, in Table B-I. The uncertainty associated with using the Martinelli formulation over the various flow regimes to obtain the magnitude of the total fluid-structure interaction is believed to be bounded by the weighting factor variation.

H. Liquid to Vapor Momentum Coupling

The uncertainty in the liquid-vapor momentum coupling has a number of contributors as shown in Table B-VI. The phenomena is treated in SIMMER-II as an interaction between a gas stream and a single liquid or solid particle. An attempt is made to account for the presence of a number of droplets or particles through an inverse dependence of the coupling on vapor volume fraction raised to an exponent (y_{18} in Table B-I). The single particle interaction is uncertain in terms of the appropriate drag coefficient to use. The effects of droplet distortion and size distribution are believed to dominate this uncertainty. The uncertainty range was selected at $\pm$ 2 times the nominal value of 0.5. The uncertainty in the treatment of multiple droplet situations and particularly the low vapor volume fraction regimes is believed to be large. Recent experiments with particle beds indicate that the interference effect should be characterized by a terms like $1/\alpha^5$ where α is the vapor volume fraction. Droplet deformation and flow regime effects could reduce this interference substantially. A film flow regime with no wavelet formation

TABLE B-VI

CONTRIBUTORS TO THE UNCERTAINTY IN LIQUID-VAPOR MOMENTUM COUPLING

	Contributors	Remarks
1.	Reynolds number dependency	Drag coefficient is overestimated in the transition region between laminar and turbulent flow. Dependency of C_D on Re in the turbulent regime is not modeled.
2.	Multiparticle environment	Boundary layer interference effects.
3.	Particle size distributions	Drag force to mass ratio changes with size.
4.	Immiscible liquids	SIMMER-II does not allow liquid-liquid relative motion.
5.	Droplet distortion	Deviations from spherical will change C_D.
6.	Flow regime	

would have a relatively small interfield drag and can be considered to be more characterized as a regime of small liquid-liquid interference. Flooding regimes would be more characterized by massive interference. We have selected a range for the exponent, α, from 0 to 5 for this study. No attempt was made to couple the exponent to the flow regime parameter x_1 in Table B-I because many different flow regimes may occur concurrently in different regimes of the problem. The x_1 variation is defined primarily as applying to the flow regimes that may exist in the upper core structure.

I. Liquid Breakup-Fluid Dynamic

The critical Weber number is used in SIMMER-II to determine droplet sizes resulting from fluid dynamic breakup. The contributors to the uncertainty in a characteristic size from fluid dynamic breakup are given in Table B-VII. The critical Weber number has been found to vary widely in various types of flow fields. In a rapidly accelerating flow such as occurs when a shock wave passes through the two-phase fluid, the critical Weber number tends to be on the order of 6 (formulated on the basis of droplet radius). In quasistatic flows it is on the order of 11. The potential exists in multicomponent flow for droplets of one type to be accelerated relative to droplets of a different type. Thus collisions can take place with the possibility of mechanically induced breakup. This is a difficult contributor to quantify but because it could be large we have used it to set the minimum of the range. A similar situation may occur when a distribution of sizes exists. The uncertainty in selecting the single characteristic size is treated explicitly in a separate parameter, y_{22}. We have selected a critical Weber number range of 0.2 to 2 times the nominal value of 22 in order to envelope the uncertainties.

J. Multicomponent Size Distributions in Single Phase Liquid Regions

The fluid dynamic and flashing breakup models are inoperative in single phase liquid cells in the SIMMER-II treatment. In multicomponent single phase liquid cells, the possibility for large energy exchange rates exists because of the imposed contact of the materials. The rates depend strongly on the contact area between the components. To prevent these contact areas from becoming unrealistically small, a maximum liquid droplet size is input to SIMMER-II. In general the liquid dispersions in these cells will be determined by the level of turbulence, strength of shear forces, parent configuration such as can wall thickness before melting and droplet sizes prior to

TABLE B-VII

CONTRIBUTORS TO THE UNCERTAINTY IN FLUID DYNAMICS BREAKUP OF LIQUID

	Contributors	Remarks
1.	Type of flow	Highly accelerating or quasistatic.
2.	Size distribution characterization	Which size characterizes the distribution.
3.	Multicomponent	Collisions between different droplets.
4.	Number density	Interference effects.
5.	Material properties	Particularly surface tension.
6.	Viscous flows	Breakup by shear forces.

setting up the single phase liquid situation. The liquid-liquid contact is particularly important in the core region where liquid fuel to liquid steel heat transfer is involved. In general it appears that for this type of problem other regions in which important heat transfer occurs are two-phase and therefore subject to the other breakup modes. This is again a difficult uncertainty to quantify. We have selected the range as $\pm$ 2 times the nominal maximum droplet radius of 0.001 m based mainly on the typical droplet sizes observed in adjacent two-phase, multicomponent cells in the core region.

K. Liquid Coalescence

The droplet coalescence model in SIMMER-II is based on a conceptual view of liquid droplets continually colliding with each other. The contributors to the overall uncertainty in this phenomena are listed in Table B-VIII. Each contributor is believed to be large. The efficiency of coalescence when a collision occurs could be uncertain by an order of magnitude. The magnitude of the random velocities could also be uncertain by an order of magnitude. The droplet size distribution contributes to this random velocity uncertainty as do the local flow characteristics -- turbulence, structures, etc. Another major contriburor is the flow regime. If the liquid is separated from the vapor in the flow field, the liquid droplets will be in closer proximity than if uniformly dispersed. This would lead to enhances coalescence. We believe that the coalescence phenomena is uncertain by at least an order of magnitude in each direction relative to the nominal model.

TABLE B-VIII

CONTRIBUTORS TO THE UNCERTAINTY IN LIQUID COALESCENCES

	Contributors	Remarks
1.	Size distribution characterization	Is treated explicitly as uncertainty y_2.
2.	Coalescence efficiency	Probability of coalescences per collision.
3.	Magnitude of random velocity	Local turbulence, acceleration, etc.
4.	Influence of structure	Induced directional changes, flow field characteristics, etc.
5.	Flow regimes	Controls the proximity of liquid droplets.
6.	Material properties	Particularly surface tension.

L. Characterization of Particle and Droplet Size Distributions

The uncertainty associated with the selection of a single particle of droplet size to represent a distribution is difficult to determine because the exchange processes depend on droplet size in different ways. For example liquid-liquid heat transfer is approximately proportional to $1/r^2$, turbulent liquid-vapor heat transfer goes as $1/r^{0.2}$, turbulent liquid-vapor drag goes as $1/r$, laminar liquid-vapor drag goes as $1/r^2$, etc. It is impossible therefore to select a single size from a distribution which will produce exchange rates that are consistent with those obtained by integrations over the distribution. A further difficulty arises because the inventories of transported entities tend to be associated with the larger droplets or particles whereas the transport rates are controlled by the smaller sizes. Thus if one could select a characteristic size that preserves the distributional rates, the tendency would be to overestimate the integrated transport with respect to time. The effect is to artificially shift the inventories to the smaller size particles. With these difficulties in mind we elected to simply force a variation on the characteristic sizes that are presently used in SIMMER-II in an attempt to discover the strength of this uncertainty on the energetics. Therefore were selected a multiplicative variation of 0.5 to 2.

The uncertainties in the characteristic sizes for solid fuel and solid steel particles, y_{23} and y_{24} in Table B-I, are similar to those for the

liquids discussed above. Addition uncertainty is involved here, however, in the selection of the characteristic sizes that are input to SIMMER-II. Nevertheless we have elected to follow the approach above and attempt to discover the existence of a strong influence on the results. Therefore a range of 0.5 to 2 times the nominal input values was selected.

M. Fuel and Steel Interaction with Sodium

From the analysis of the best-estimate calculations it appeared that the fuel to sodium heat transfer in the region above the subassemblies is fundamentally important in the production of kinetic energy. The expansion appears to be driven totally by sodium vapor. The processes governing the production of sodium vapor are highly uncertain and must be dealt with in this study. The uncertainty in the energy exchange to the sodium is related to both the specific heat transfer rates and the mixing mechanics. The uncertainty in the specific heat transfer rates was considered previously in stems y_8, y_9, y_{10} and y_{11} of Table B-I. Uncertainties affecting particle size are also considered separately. The one remaining uncertainty to be considered is mixing mechanics.

Separate studies with SIMMER-II indicated that mixing of liquid components which are initially unmixed tends to be limited by the SIMMER-II fluid dynamics treatment to one or two interfacial mesh cells. Thus one way to vary the mixing mechanics in SIMMER-II is the vary the cell structure in the mixing region. If one calculates the penetration distance for various droplets and particles under various conditions of size and velocity into a liquid sodium interface, it is found that these distances vary from a few centimeters to several tens of centimeters. This basis was used to set the uncertainty range for mixing. The cells size was permitted to vary linearily from about .05 to .30 meters.

N. Vapor Pressures

The remaining three uncertainty ranges that need to be specified are associated with the vapor pressure of the three primary reactor materials. SIMMER-II uses a simple exponential expression to relate vapor pressure to liquid temperature. In attempting to select the constants for these expressions, it becomes apparent that considerable scatter exists in the data and/or theories for vapor pressures, particularly for fuel and steel. We view these scatter bands as indications of the uncertainties in the vapor

pressures. We attempted therefore to select a range for the multiplicative constant, p^* in the expression

$$p = p^* e^{-T^*/T_\ell} ,$$

that would force p to have the apparent scatter in the data. The ranges for fuel and steel were taken as 0.5 to 4 times the nominal values for the p^*'s. The uncertainty in the sodium vapor pressure is much smaller; on the order of $\pm$ 10%.

APPENDIX C
DESIGN OF 15 SIMMER-II RUNS WITH VARIED MODELING ASSUMPTIONS

The ranges of possible variation for SIMMER-II input parameters, as described in Appendix B, represent the degree of uncertainty in the SIMMER-II representation of the phenomena involved. In this section, the design of 15 SIMMER-II computer runs is described. The input values used in these runs were selected from the ranges of variation according to the procedure outlined below.

Since wide variations of 25 independent input parameter values are specified, there exists a large number of different combinations of possible SIMMER-II input sets. For example, if only two values are permitted for each input parameter (i.e. the maximum of the range of variation and the minimum), there are 2^{25}, or over 30 million different combinations. Clearly, all possible combinations cannot be used. Therefore, an efficient procedure for choosing input sets is needed. The procedure used in this study is efficient in the sense that a small number of input sets and SIMMER runs (i.e. 15) are needed.

Along with the selection of ranges of input value variation one must specify the likelihood of choosing given values in the ranges (i.e. probability distributions). These probability distributions govern the selection of values in a systematic way. In order to permit equal chances of selecting values from any part of a range, uniform probability distributions were used in this study. A distribution is described with respect to a linear scale for small variation ranges (e.g. $\pm$ 25% of nominal) and a logarithmic scale for large variations (e.g. order of magnitude). Table B-I indicates the scale used for each input variation.

Several methods are available for selecting input values according to the probability distributions. These include (1) random selection, (2) Latin Hypercube Sampling, or LHS,[12,13] and (3) a version of randomized fractional replication.[14] The latter was used in this study, but all three are described below because they are all related. All of these methods require changing each input parameter value in each computer run.

Random selection for an individual input parameter is performed using a string of randomly generated numbers ranging from 0 to 1. The string can

be generated using a random number generator on a computer or scientific calculator, or can be referenced from random number tables in standard mathematics handbooks. If 15 computer runs are to be performed, the string is of length 15. One string is needed for each of the 25 independent input variations. A random number of 0.45, for example, indicates that the 45^{th} percentile value from the probability distribution for the input parameter should be selected. For a particular variation range from 0-10, for example, the 45^{th} percentile is 4.5, given a uniform probability distribution on a linear scale.

This method provides an acceptable way to choose input sets and is used in many other applications, but there are problems when the number of runs to be performed is as small as 15. The method is likely to result in a biased set of input value selections, because there is a good chance (i.e. 0.15) of choosing as many as ten of the percentile values above the 50% mark. Further, it is possible to find two or more of the 15 percentile values to be nearly equal. This is somewhat inefficient, as it is desirable to use different values of each input parameter in each run, where possible.

The method of LHS eliminates the problem of bias. This is accomplished by selecting the first of the 15 random percentiles (e.g. 45^{th}) and eliminating from further consideration the subrange, or $1/15^{th}$ of the number line, around that percentile value (e.g. 40^{th} to 47^{th}). This is repeated for all successive selections, guaranteeing even coverage of the range. This was the method used in previous LWR applications. Still, it is possible to find two percentile values close together by selecting one toward the high end of a subrange and another towards the low end of the next highest subrange.

The method based on fractional replication eliminates the problem of bias and the possibility of selecting two similar percentile values. The first step of the method is identical to the random selection technique. It requires random selection of 15 values. This fixes the order in which values are to be selected in the 15 runs. For example, if the lowest percentile selection occurs on the 5^{th} of the 15 values, the lowest value of that input parameter will be used in run number 5.

Once the order is decided, the percentile selections are replaced with equally-spaced percentile values, but in the same order as the original random string. For example, the following random string of length 15:

.13 .21 .99 .00 .60 .91 .97 .35 .39 .17 .36 .71 .98 .72 .24,

is replaced by:

.07 .21 1.00 .00 .57 .79 .86 .36 .50 .14 .43 .64 .93 .71 .29,

wherein the numbers are in the same order as the previous sequence, but their values are evenly spaced. In this example for a particular input parameter, the 7^{th} percentile value is used in run 1, 21^{st} in run 2, 100^{th} in run 3, and so on. This process is repeated for all 25 input parameters. The values used for the 15 runs are listed in Table C-I where the input variable designations refer to the y's in Table B-I.

It can be proven using methods of order statistics[15] that the equally-spaced percentile values represent the most probable configuration of the random selection technique. That is, if an infinite number of random strings of length 15 are selected, the most-occuring lowest-percentile value will be zero, the next lowest will be the 7^{th} percentile, and so on. In general, for strings of length n, the most probable value for the i^{th} lowest percentile selection (i = 1,...,n) is 100(i-1)/(n-1).

TABLE C-I

INPUT DATA SETS FOR THE POSTDISASSEMBLY ENERGETIC SENSITIVITY STUDY

Input Variable \ Run #	1	2	3	4	5
y_1 = 1	0.00349	0.0183	0.00306	0.00297	0.00170
y_2 = 2	0.00103	0.0149	0.00599	0.000249	0.0111
. = 3	0.0500	0.0168	0.0205	0.0226	0.0138
. = 4	0.0368	0.059	0.0431	0.0197	0.00897
. = 5	0.0981	0.0861	0.0963	0.0986	0.0948
= 6	0.693	0.316	0.949	0.231	0.370
= 7	0.126	0.502	0.159	0.795	0.631
= 8	164	124	93.5	286	17.5
= 9	0.535	5.00	0.175	0.132	1.24
= 10	0.631	0.200	0.317	2.51	0.399
= 11	0.252	1.99	0.502	3.97	3.16
= 12	0.240	0.0684	0.0427	0.175	0.205
= 13	0.00563	0.00708	0.00252	0.00891	0.0100
= 14	0.128	0.0584	0.240	0.0684	0.150
= 15	0.00563	0.00708	0.00252	0.00891	0.0100
= 16	0.141	0.571	0.221	0.117	0.286
= 17	0.820	0.371	0.250	0.610	0.453
= 18	4.29	2.14	1.79	1.43	0.36
= 19	19.3	10.0	31.7	26.9	13.9
= 20	0.00149	0.000552	0.000673	0.000743	0.00200
= 21	3.73	5.18	1.00	0.139	1.39
= 22	0.673	2.00	1.10	1.35	0.552
= 23	$7.43(10^{-5})$	$1.10(10^{-4})$	$2.00(10^{-4})$	$8.20(10^{-5})$	$1.22(10^{-4})$
= 24	0.00149	0.00122	0.00181	0.00164	0.00110
= 25	0.3048	0.1524	0.0508	0.0762	0.0870857
= 26	$8.35(10^{10})$	$2.36(10^{11})$	$3.69(10^{11})$	$7.20(10^{10})$	$5.76(10^{11})$
= 27	$2.55(10^{11})$	$5.35(10^{11})$	$1.05(10^{11})$	$1.41(10^{11})$	$1.22(10^{11})$
= 28	$4.03(10^{9})$	$3.54(10^{9})$	$3.60(10^{9})$	$3.87(10^{9})$	$3.71(10^{9})$

TABLE C-I (cont)

Input Variable \ Run #	6	7	8	9	10
1	0.0127	0.0613	0.000987	0.0308	0
2	0.0345	0.0267	0.00143	0.0335	0.0250
3	0.0336	0.0276	0.0250	0.0125	0.0305
4	0.0504	0.0269	0.0144	0.0105	0.0690
5	0.0807	0.06270	0.0990	0.0732	0.0900
6	0.169	0.270	0.197	0.811	0.144
7	0.0634	0.399	0.252	0.317	0.200
8	70.7	13.2	40.4	378	216
9	2.16	2.86	2.78	0.707	0.231
10	0.795	1.58	0.502	1.99	3.97
11	0.631	0.200	1.26	2.51	1.58
12	0.080	0.128	0.0584	0.0936	0.150
13	0.00355	0.00399	0.00282	0.00200	0.00224
14	0.109	0.0365	0.175	0.0312	0.0800
15	0.00355	0.00399	0.00282	0.00200	0.00224
16	0.643	0.786	0.100	0.714	0.500
17	1.00	0.336	0.743	0.276	0.305
18	4.64	2.86	3.93	3.21	0.71
19	44.0	22.8	5.19	11.8	7.21
20	0.00110	0.00050	0.000820	0.00135	0.00122
21	0.193	0.720	1.93	0.268	7.20
22	1.49	0.500	1.81	1.00	0.743
23	$1.64(10^{-4})$	$9.06(10^{-5})$	$6.10(10^{-5})$	$5.00(10^{-5})$	$1.81(10^{-4})$
24	$6.73(10^{-4})$	$8.20(10^{-4})$	$6.10(10^{-4})$	$5.00(10^{-4})$	$9.06(10^{-4})$
25	0.0508	0.0677333	0.0508	0.12192	0.3048
26	$1.12(10^{11})$	$2.74(10^{11})$	$1.51(10^{11})$	$1.30(10^{11})$	$2.04(10^{11})$
27	$3.43(10^{11})$	$7.77(10^{10})$	$4.63(10^{11})$	$2.96(10^{11})$	$2.20(10^{11})$
28	$3.38(10^{9})$	$3.81(10^{9})$	$4.14(10^{9})$	$3.76(10^{9})$	$3.92(10^{9})$

TABLE C-I (cont)

Input Variable \ Run #	11	12	13	44	15
1	0.000438	0.0166	0.0766	0.127	0.0354
2	0.00622	0	0.0462	0.0358	0.142
3	0.0186	0.0152	0.0453	0.0410	0.0371
4	0.0230	0.0168	0.0123	0.00767	0.0315
5	0.0973	0.0928	0.0482	0	0.0280
6	0.506	0.123	1.11	0.592	0.433
7	0.0503	0.100	0.0400	1.0	0.0797
8	10.0	53.5	500	30.6	23.1
9	0.404	1.64	0.306	0.935	0.100
10	3.16	1.00	0.252	5.00	1.26
11	0.399	0.317	1.00	0.795	5.00
12	0.0365	0.0500	0.0312	0.0267	0.109
13	0.00631	0.00447	0.00502	0.00317	0.00795
14	0.0427	0.0500	0.0267	0.0936	0.205
15	0.00631	0.00447	0.00502	0.00317	0.00795
16	0.175	0.376	0.857	1.00	0.928
17	0.673	0.906	0.552	0.500	0.410
18	1.07	2.50	0	3.67	5.00
19	16.4	37.3	4.40	8.50	6.11
20	0.000610	0.00164	0.00100	0.000906	0.00181
21	0.100	10.0	0.373	2.68	0.518
22	0.610	1.64	0.906	0.820	1.22
23	$5.52(10^{-5})$	$1.00(10^{-4})$	$1.49(10^{-4})$	$1.35(10^{-4})$	$6.73(10^{-5})$
24	$1.35(10^{-3})$	$7.43(10^{-4})$	$1.00(10^{-3})$	$2.00(10^{-3})$	$5.52(10^{-4})$
25	0.3048	0.2032	0.06096	0.1016	0.00554182
26	$1.76(10^{11})$	$4.28(10^{11})$	$3.18(10^{11})$	$9.69(10^{10})$	$4.96(10^{11})$
27	$3.99(10^{11})$	$9.02(10^{10})$	$6.70(10^{10})$	$1.89(10^{11})$	$1.63(10^{11})$
28	$3.49(10^{9})$	$3.98(10^{9})$	$4.08(10^{9})$	$3.44(10^{9})$	$3.65(10^{9})$

APPENDIX D
ANALYSIS OF VARIATIONS AMONG RESULTS OF 15 SIMMER-II RUNS

The runs described in Appendix C were performed and resulted in variations in key output quantities of SIMMER-II. These variations are analyzed in this section.

The output quantities used in this study as indicators of accident energetics include maximum system kinetic energy, head impulse, and pressures calculated at key locations within the reactor vessel. The "maximum values" are the largest observed in the time history of individual calculations. The maximum system kinetic energy prior to head impact is a measure of the damage potential for the primary system. Table D-I summarizes of output values for the 15 SIMMER-II runs.

The kinetic energy varied a factor of 8 from minimum to maximum (2.5-20 MJ). None of the other outputs listed in Table D-I varied by more than this factor. Table D-II shows the values of the output quantities for each of the 15 runs.

The objective of this analysis is to discover which, if any, of the input parameter variations correlates well with the variation observed in system kinetic energy. The purpose of this approach is to reveal to which phenomenological uncertainties the SIMMER-II results are most sensitive. Note that the conclusions based on this analysis are fully dependent on the sizes of the 25 input variations, the version of SIMMER used, and the particular problem description. The conclusions are also dependent on the probability distributions selected for each input variation and the fact that there are 25 independent variations, because this information determines the likelihood of selecting certain combinations of phenomenological variations in the 15 runs. For example, the selection of an input set with the worst-case (i.e. most conservative) value for each of the 25 input parameters is highly unlikely.

The procedure is to calculate a correlation coefficient between kinetic energy and each of the 25 input variations in turn. Then the best correlated input among the 25 is tested for significance of the correlation. That is, the magnitude of the correlation coefficient is tested to determine the chance that the apparent correlation could be

TABLE D-I

SUMMARY OF RESULTS OF 15 SIMMER-II CALCULATIONS

	Max. KE (MJ)	Impulse to Head (MNs)	Max. Press. at Head (MPa)	Max. Avg. Press. at Head (MPa)	Core Press. at Impact (MPa)	Peak FCI Zone Press. (MPa)	Avg. FCI Zone Press. (MPa)	Time of Peak Press.* (s)	Time of Impact (s)
Average	8.30	1.04	5.64	3.27	1.39	2.08	1.56	0.08	0.24
Std. Dev.	4.50	0.32	1.35	1.03	0.68	1.03	0.77	0.03	0.07
Maximum	20.57	1.79	8.70	5.74	3.08	5.09	3.60	0.13	0.41
Minimum	2.52	0.57	2.72	1.73	0.76	0.80	0.62	0.03	0.14
Key Input Sensitivity	y_{26}	y_{26}	y_{26}	y_{26}	y_{26}	y_{26}	y_{26}	y_{26}	y_{26}
S-Score	61	59	51	57	77	49	51	-49	-41
Confidence in Correlation	97%	96%	86%	94%	99%	82%	86%	82%	78%

*First Peak

TABLE D-II

RESULTS OF 15 SIMMER-II CALCULATIONS

Case No.	Max. KE (MJ)	Impulse to Head (MNs)	Max. Press. at Head (MPa)	Max. Avg. Press. at Head (MPa)	Core Press. at Impact (MPa)	Peak* FCI Zone Press. (MPa)	Avg. FCI Zone Press. (MPa)	Time of Peak* Press. (s)	Time of Impact (s)
1	4.77	0.82	4.52	2.66	0.80	1.68	1.03	0.130	0.250
2	7.23	0.93	4.71	3.06	1.47	1.78	1.38	0.070	0.240
3	14.15	1.41	6.88	4.52	2.18	3.20	2.56	0.040	0.160
4	2.52	0.57	2.72	1.73	0.76	0.80	0.62	0.110	0.410
5	10.01	1.28	5.90	3.87	2.10	2.17	1.95	0.060	0.210
6	9.03	1.12	5.65	3.50	1.05	2.13	1.61	0.070	0.220
7	5.07	0.68	4.61	2.00	0.85	1.03	0.88	0.080	0.310
8	7.50	1.07	5.80	3.40	1.02	2.34	1.61	0.050	0.190
9	4.77	0.76	4.95	2.37	0.76	1.19	0.88	0.080	0.280
10	5.76	0.89	5.66	2.98	1.08	1.69	1.18	0.080	0.230
11	8.45	1.10	5.35	3.48	1.26	1.84	1.56	0.100	0.210
12	20.57	1.79	8.70	5.74	3.08	5.09	3.60	0.060	0.140
13	8.59	1.19	6.34	3.57	1.66	1.73	1.56	0.080	0.250
14	5.00	0.74	5.73	2.31	0.82	0.94	0.85	0.130	0.360
15	11.04	1.26	7.02	3.86	1.98	2.62	2.10	0.030	0.190

*First Peak

simply a lucky configuration of random noise. Note that there is a finite probability of finding two entirely independent sequences from independent sources and observe some apparent correlation purely by chance.

Various correlation methods are available. The most commonly used in engineering application are linear, exponential, logrithmic, and power regressions. In these methods, the analyst attempts to find to what degree the data conforms to the functional form being tested. None of those methods are suitable for the present analysis because they are all specifically related to functional forms. Rather than discovering the functional forms of input- output relationships, the purpose in the present analysis is simply to find monotonic relationships, regardless of functional form.

A correlation method that tests only for monotonicity is the Kendall's tau method.[16,17] The procedure is to look for like patterns of variation between two sequences of numbers, for example, $(x_1, \ldots, x_n)$ and $(y_1, \ldots, y_n)$. This basically involves comparing each possible pair of values in the first sequence (e.g. x_2, x_5) with its corresponding pair in the second sequence (y_2, y_5), scoring +1 if the first member of each pair is smaller (or larger) than the second in each pair ($x_2 > x_5$ and $y_2 > y_5$, or $x_2 < x_5$ and $y_2 < y_5$), and scoring -1 otherwise ($x_2 > x_5$ and $y_2 < y_5$, or $x_2 < x_5$ and $y_2 > y_5$). These are referred to as positive and negative scores, respectively. For sequences of length n there are n(n-1)/2 possible pair combinations, and the total score, S, can be between -n(n-1)/2 and n(n-1)/2. Hence, the Kendall's tau is defined:

$$\tau = \frac{S}{n(n-1)/2} \quad .$$

Note that for perfectly positively correlated sequences the tau value is +1, and for perfectly negatively correlated sequences it is -1. This is consistent with the more common correlation methods. Values of tau between these two extremes indicate less than perfect correlation, and values around zero indicate randomness i.e., no correlation.

The best correlated input sequence in Table C-I with the kinetic energy sequence in Table D-II is y_{26}; the parameter in the fuel equation of state

relating vapor pressure to saturation temperature. The S score for this correlation is 61, counting ties as -1 (τ = 61/105 = 0.58). The significance of S scores can be determined from statistical tables.[16,17] The chance of selecting two independent sequences of length 15 at random and obtaining S = 61 is found in the tables to be only 0.0014, indicating that the apparent correlation is probably not just random noise. However, it must be noted that this correlation is the best among 25 correlations, which increases the chance of finding apparently well correlated, but random sequences. The significance of the S = 61 score must be re-evaluated.

The chance that any one of the 25 correlations has an S score less than 61 is 1-0.0014, or 0.9986, if the sequences are truely random and independent of the output sequence of kinetic energy values. The chance that all 25 S scores are less than 61 is then 0.9986^{25}, or 0.97. Hence, the chance that the best correlated of the 25 correlations has S = 61 is 1-0.97, or 0.03. This 3% chance translates to 97% confidence in the rejection of the claim that kinetic energy and y_{26} are not correlated.

This result warrents qualititive discussion, as few people have an understanding of the meaningfulness of S score values. As previously stated, tau values of unity indicate perfect monotonic correlation; hence, the value of 0.58 for the above S score of 61 indicates positive, although less than perfect, correlation. The reason is that lesser sensitivities of the kinetic energy to other input variations still show up as noise, because the y_{26} sensitivity is not strong enough to completely dominate the results. This is apparent in the scatter in the results shown in Fig. D-1, which shows the general trend of the y_{26} - kinetic energy relationship and illustrates the degree of noise resulting from lesser sensitivities to the other 24 input variations.

It can be seen from Fig. D-1 that the correlation depends on the size of the y_{26} variation. If the variation were smaller than ½ to 4 times nominal, the size of the bandwidth for the random noise (i.e. the degree of vertical deviation of the scattered points in Fig. D-1 from a common, monotonic curve) could become larger than the y_{26} variation, and the correlation would no longer be apparent. Further if the size of other input variations were increased, this could increase the noise bandwidth and mask out the appparent y_{26} correlation.

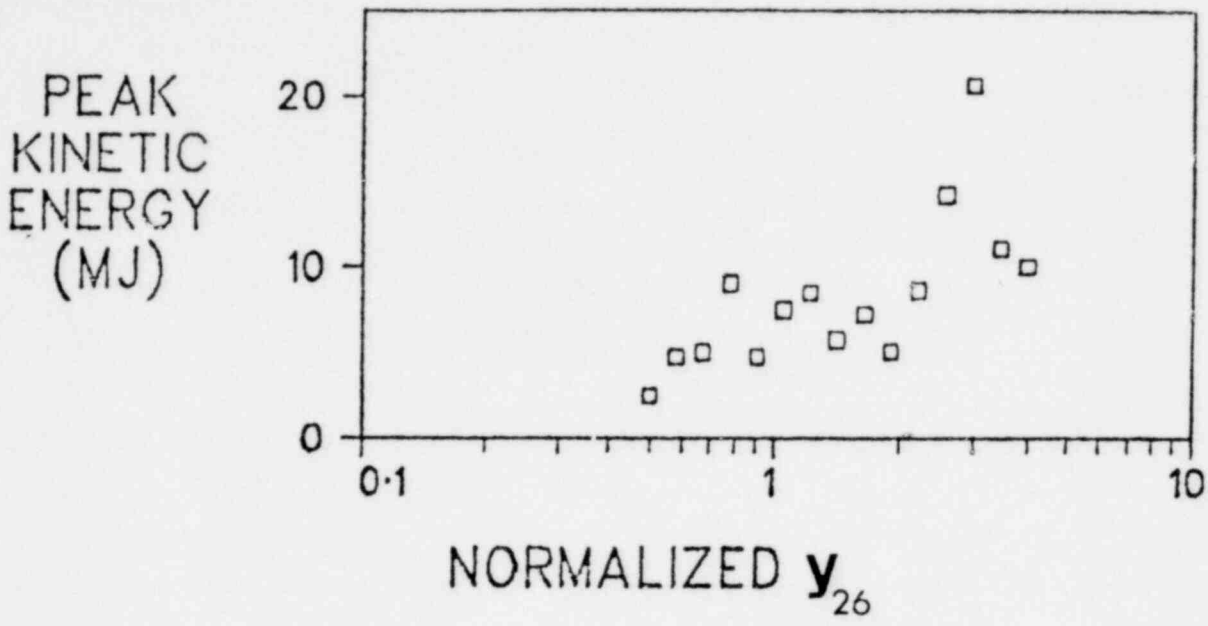

Fig. D-1.
Scattergram of y_{26} and kinetic energy.

To determine the impact on the sensitivity analysis of decreasing the y_{26} variation to ½ to about 2 times nominal, the results of four SIMMER-II runs (3, 5, 12, and 15) were not considered, leaving only 11 runs in which y_{26} was less than 2.2 times nominal. This reduced the number of possible pair combinations to 11(11-1)/2, or 55.

The best S scores were found for two of the 25 correlations - the multi-component stratification parameter (x_2 in Table B-I) and liquid fuel-to-liquid steel heat transfer multiplier, (y_7 in Table B-I). The S scores were +25 and -25, respectively. The confidence in each correlation is 97.5%, when considered individually, but only 53% when considered as the best of 25 possible correlations (i.e., $.975^{25}$ = .53). Hence, no single input variation was found to influence the kinetic energy in the low y_{26} region (i.e., low energy).

However, when only the pairs wherein x_2 increased from the first run to the second run and y_7 decreased, kinetic energy was observed to increase from the first run to the second in 33 of the remaining 40 pairs. The confidence in the multiple correlation of x_2 and y_7 with kinetic energy is

99.7%. (S scores cannot be determined for multiple correlations using available tables. The confidence in the correlation was determined by calculating S scores for comparing x_2 and y_7 with 1285 other sequences chosen at random. Only 3 of these had higher S scores than the correlation with kinetic energy.

When only pairs wherein x_2 increased, y_7 decreased, and the liquid fuel-to-liquid sodium heat transfer multiplier (y_8 in Table B-I), decreased, kinetic energy was observed to increase in 20 of the remaining 21 pairs. The confidence in the correlation is greater than 99.5%. (None of the S scores for comparing x_2, y_7, and y_8 with 1285 random sequences equaled or exceeded 20).

Large x_2 implies decreased liquid fuel-to-structure heat transfer (stratification favors liquid steel, rather than liquid fuel, in contact with structure) and small y_7 and y_8 imply the same. Further, large x_2, small y_7, and small y_8 correlate with higher system kinetic energy. Therefore, it appears that the slower that heat can be removed from liquid fuel, the higher will be the kinetic energy. This is the main sensitivity at low energies.

The situation is different at higher energies. For this analysis, only those runs with y_{26} values from about 2 to 4 times nominal were considered. There are six runs with y_{26} greater than 1.9 times nominal, reducing the number of possible pair combinations to 6(6-1)/2 or 15. The droplet size distribution multiplier (y_{22} in Table B-I) was found to be the best correlated input variation for high y_{26} values (high energy), with an S score of 11. The confidence in the correlation is 99%, when considered as a single correlation, but is only 78% when considered as the best of 25 correlations ($0.99^{25} = 0.78$).

Because large y_{22} implies larger droplet sizes, the coalescence multiplier (y_{21} in Table B-I) was considered in further analysis. It was found that in 9 pairs, both y_{22} and y_{21} increased. In each of these, kinetic energy also increased. The confidence in this correlation in greater than 99%. (Only one of the S scores for comparing y_{22} and y_{21} with 1285 random sequences was as large as 9.)

Large y_{22} and y_{21} imply larger droplet sizes. These imply reduced coupling between the liquid and vapor fields, reduced vaporization/condensation, and slower liquid-liquid heat transfer. Because heat transfer

rates were already determined not to impact sensitivities at high energies, it appears that kinetic energy is sensitive to either interfield momentum coupling and/or phase change rates.

The selection of the input parameter values was random as was previously described; therefore, assume that there is a probability P that the energy will be less than or equal to 20 MJ in any given SIMMER-II run. Thus, the probability that the energy would not have exceeded 20 MJ in the 15 runs is P^{15}. This is used to determine how large P must be in order for there to have been an 0.5 probability of exceeding 20 MJ in 15 runs and an 0.5 probability of not:

$$0.5 = P^{15} \text{ or } P = 0.95$$

Therefore, the best estimate is that there is only a 5% chance of exceeding 20 MJ in another run.

A more conservative estimate is obtained by finding how large P must be in order for it to have been unlikely not to have exceeded 20 MJ in 15 runs. "Unlikely" is quantified as 5% chance (which translates to 95% statistical confidence in the result). Thus:

$$0.05 = P_{cons}^{15} \quad \text{or } P_{cons} = 0.82 ,$$

and the conservative estimate is that there could be as high as an 18% chance of exceeding 20 MJ in another run.

With regard to the other output quantities listed in Tables D-I and D-II, all were found to correlate well with the variations in y_{26} and kinetic energy.

REFERENCES

1. C. R. Bell, P. B. Bleiweis, J. E. Boudreau, F. R. Parker, and L. L. Smith, "SIMMER-I: An Sn, Implicit, Multifield, Multicomponent, Eulerian, Recriticality Code for LMFBR Disrupted Core Analysis," Los Alamos Scientific Laboratory report LA-NUREG-6467-MS (January 1977).

2. C. R. Bell and J. E. Boudreau, "Application of SIMMER-I to the Postdisassembly Fluid Dynamic Behavior within an LMFBR Reactor Vessel," Los Alamos Scientific Laboratory report to be published.

3. J. F. Jackson, and M. G. Stevenson, "Nuclear Reactor Safety Quarterly Progress Report April 1-June 30, 1978," Los Alamos Scientific Laboratory report NUREG/CR-0385 LA-7481-PR (October 1978).

4. L. L. Smith, "SIMMER-II: A Computer Program for LMFBR Disrupted Core Analysis," Los Alamos Scientific Laboratory report NUREG/CR-0453 LA-7515-M (October 1978).

5. M. D. McKay, J. W. Bolstad, and D. E. Whiteman, "An Application of Statistical Techniques to the Analysis of Reactor Safety Codes," Proc. ANS Topical Mtg., Probabilistic Analysis of Nuclear Reactor Safety, (Los Angeles, California, 1978), pp. ii-9.

6. R. D. Burns III, Los Alamos Scientific Laboratory, personal communication, September 27, 1977.

7. R. D. Burns III and L. B. Luck, "Statistical Analysis of SIMMER-II Results," ANS Trans. 28 (1978) p. 513.

8. R. D. Burns III and J. H. Scott, "Statistical Analysis of Seventeen TREAT Experiments," accepted for presentation, ANS 1978 Winter Meeting, Washington, D.C., November, 1978.

9. J. F. Jackson and M. G. Stevenson, "Nuclear Reactor Safety Quarterly Progress Report October 1-December 31, 1978," Los Alamos Scientific Laboratory report to be published.

10. J. Marchaterre, et al., "Work-Energy Characterization for Core-Disruption Accidents," Proc. Int. Mtg. on Fast Reactor Safety and Related Physics, October 5-8, 1976 (Chicago, Illinois, 1976).

11. J. F. Jackson and M. G. Stevenson, "Nuclear Reactor Safety Quarterly Progress Report January 1-March 31, 1977," Los Alamos Scientific Laboratory report LA-NUREG-6842-PR.

12. M. D. McKay, W. J. Conover, and D. E. Whiteman, "Report on the Application of Statistical Techniques to the Analysis of Computer Codes," Los Alamos Scientific Laboratory report LA-NUREG-6526-MS (August 1976).

13. M. D. McKay and R. J. Beckman, "A Comparison of Three Methods for Selecting Values of Input Variables in the Analysis of Output From a Computer Code," Los Alamos Scientific Laboratory report LA-UR-77-01 (1977).

14. S. Zacks, "Generalized Least Squares Estimators for Randomized Fractional Application Designs," Ann. Math. Statist. 35, pp. 696-704 (1964)

15. R. V. Hogg and A. T. Craig, Introduction to Mathematical Statistics, (Macmillian, London, 1970) Section 4.6.

16. W. J. Conover, Practical Nonparametric Statistics, (Wiley, New York, 1971) p. 249.

17. M. G. Kendall, Rank Correlation Methods, (Hafner, New York, 1955).

DISTRIBUTION

	Copies
Nuclear Regulatory Commission, R7	308
Technical Information Center, Oak Ridge, Tennessee	2
Los Alamos Scientific Laboratory	50

☆ U.S. Government Printing Office: 1979 — 677-115/192

Available from
US Nuclear Regulatory Commission
Washington, DC 20555

Available from
National Technical Information Service
Springfield, VA 22161

Microfiche $3.00

001-025	4.00	126-150	7.25	251-275	10.75	376-400	13.00	501-525	15.25
026-050	4.50	151-175	8.00	276-300	11.00	401-425	13.25	526-550	15.50
051-075	5.25	176-200	9.00	301-325	11.75	426-450	14.00	551-575	16.25
076-100	6.00	201-225	9.25	326-350	12.00	451-475	14.50	576-600	16.50
101-125	6.50	226-250	9.50	351-375	12.50	476-500	15.00	601-up	

Note: Add $2.50 for each additional 100-page increment from 601 pages up.